In-Situ Stresses and Palaeostresses around Salt Diapirs: a Structural Analysis from the Gulf of Mexico and Amadeus Basin, Central Australia

Thesis submitted in accordance with the requirements of the University of Adelaide for an Honours Degree in Geophysics.

Owen Girardi

November 2012

THE UNIVERSITY of ADELAIDE

IN-SITU STRESSES AND PALAEOSTRESSES AROUND SALT DIAPIRS: A STRUCTURAL ANALYSIS FROM THE GULF OF MEXICO AND AMADEUS BASIN, CENTRAL AUSTRALIA

IN-SITU STRESSES AROUND SALT DIAPIRS

ABSTRACT

Stable drilling directions are directly affected by the in-situ stress orientations and magnitudes involved. For example, in the Gulf of Mexico delta top normal fault stress regime, where the maximum horizontal stress (σ_H) is margin-parallel, vertical wells are most stable. However, in-situ stress orientations are deflected around salt diapirs and have major implications for horizontal drilling risks. This study assesses the deflection of in-situ stress orientations and palaeostress orientations in close proximity to salt diapirs using 3D seismic data from the Gulf of Mexico and structural field observations from the Amadeus Basin, central Australia. Seismic interpretation of salt diapirs in the Ship Shoal seismic cube (Gulf of Mexico) reveals gravitational collapse on the flanks of the salt diapirs, implying net normal displacement. This is consistent with the hypothesis that σ_H becomes locally deflected sub-parallel to the salt-sediment interface. The salt diapir in the Amadeus Basin field area is within a more complex structural setting compared to the Gulf of Mexico and is associated with a large NW-SE striking thrust fault. This implies that it has reacted to north-south shortening from the Alice Springs Orogeny. Palaeostress analysis from conjugate fracture pairs in the field area reveals a large variation in orientations for σ_1 and σ_3. However, σ_2 is consistently sub-perpendicular to bedding, thus σ_1 and σ_3 orientations are restricted to the plane of bedding. Evidence from both the 3D Ship Shoal seismic cube and the structural field data suggests that in-situ stress is deflected around salt diapirs. However, the results from the field structural analysis are dissimilar to seismic interpretation from the Gulf of Mexico. In-situ stress deflections along the flanks of salt diapirs are associated with complex perturbations. These deflections are dependent on the structural setting of each salt diapir and whether it is interpreted as active, passive or reactive.

KEYWORDS

In-situ stress; palaeostress; salt diapir; Gulf of Mexico; Amadeus Basin.

TABLE OF CONTENTS

LIST OF FIGURES

1. INTRODUCTION

In-situ stress orientations are locally deflected around salt diapirs to become sub-parallel to the interface between salt and sediment. Due to the relative magnitudes between principal stresses, net normal displacement around salt diapirs occurs and follows the interface between salt and sediment. The nature of the growth of the diapir and the geological setting (i.e. the in-situ stress regime) act as strong controls on both the relationship between the diapir and the surrounding sediment, and the associated deformational characteristics.

In-situ stress regimes in sedimentary basins are described in various literature (e.g. Bell 1996a, Bell 1996b). The orientation of maximum horizontal stress (σ_H) within sediments can be deduced from a range of both engineering techniques (e.g. borehole breakouts, hydraulic fracturing and leak off tests) and in-situ geological observations (e.g. fault characterisation and orientation, tectonic environment, folds and fractures) (Bell 1996a, Bell 1996b). The σ_H orientation in the delta top of the Gulf of Mexico, as inferred from borehole breakouts, has a mean orientation sub parallel to the passive margin (NE-SW) (Yassir and Zerwer 1997). This is also consistent with the idealised model of a delta deepwater fold-thrust belt (DDWFTB), where the gravitational collapse of a delta top generates a margin parallel σ_H orientation (King and Backe 2010, King et al. 2009).

However, the presence of active and passive salt diapirs in the delta top of the Gulf of Mexico deflects σ_H orientations away from the mean NE-SW margin parallel trend. In-

situ stress orientations are deflected parallel to the interface between salt diapirs and adjacent deltaic sediments. This is potentially caused by the contrast between the geomechanical properties of salt and adjacent sediments (King et al. 2012). These anomalies have major implications for the petroleum industry as the most stable well orientations in the delta top normal fault stress regime are usually vertical. Unless, σ_H is close to σ_V in magnitude, in which case wells deviated towards the minimum horizontal stress (σ_h) are the most stable (King et al. 2012, Bell 1996b). Outcrop analysis of deltaic sediments adjacent to salt diapirs was completed by Alsop et al. (2000) at Cape Breton Island, Nova Scotia. This study identified "drag zones", described as highly strained regions developed adjacent to the flanks of salt diapirs. These are produced when the sedimentary overburden is folded or rotated into steeply dipping attitudes sub-parallel to the diapiric walls (Figure 3) (Alsop et al. 2000). One of the most significant conclusions of this study was the observation of minor extensional fractures within the drag zones, implying that net normal displacement has occurred due to σ_H being deflected sub-parallel to the salt-sediment interface.

This study aims to use three dimensional (3D) seismic data from the Gulf of Mexico (Figure 1) and field observations in the Amadeus Basin, central Australia (Figure 2); two areas renowned for salt diapirs. I will investigate the relationships between diapirism and sediment at both seismic and outcrop resolutions. Deformation styles, fractures, fault networks and geometries of stratigraphic packages observed in the field and on seismic data are determined. Ultimately, this provides palaeostress and in-situ stress orientations as well as some relative magnitudes within sediment along the flanks of salt diapirs.

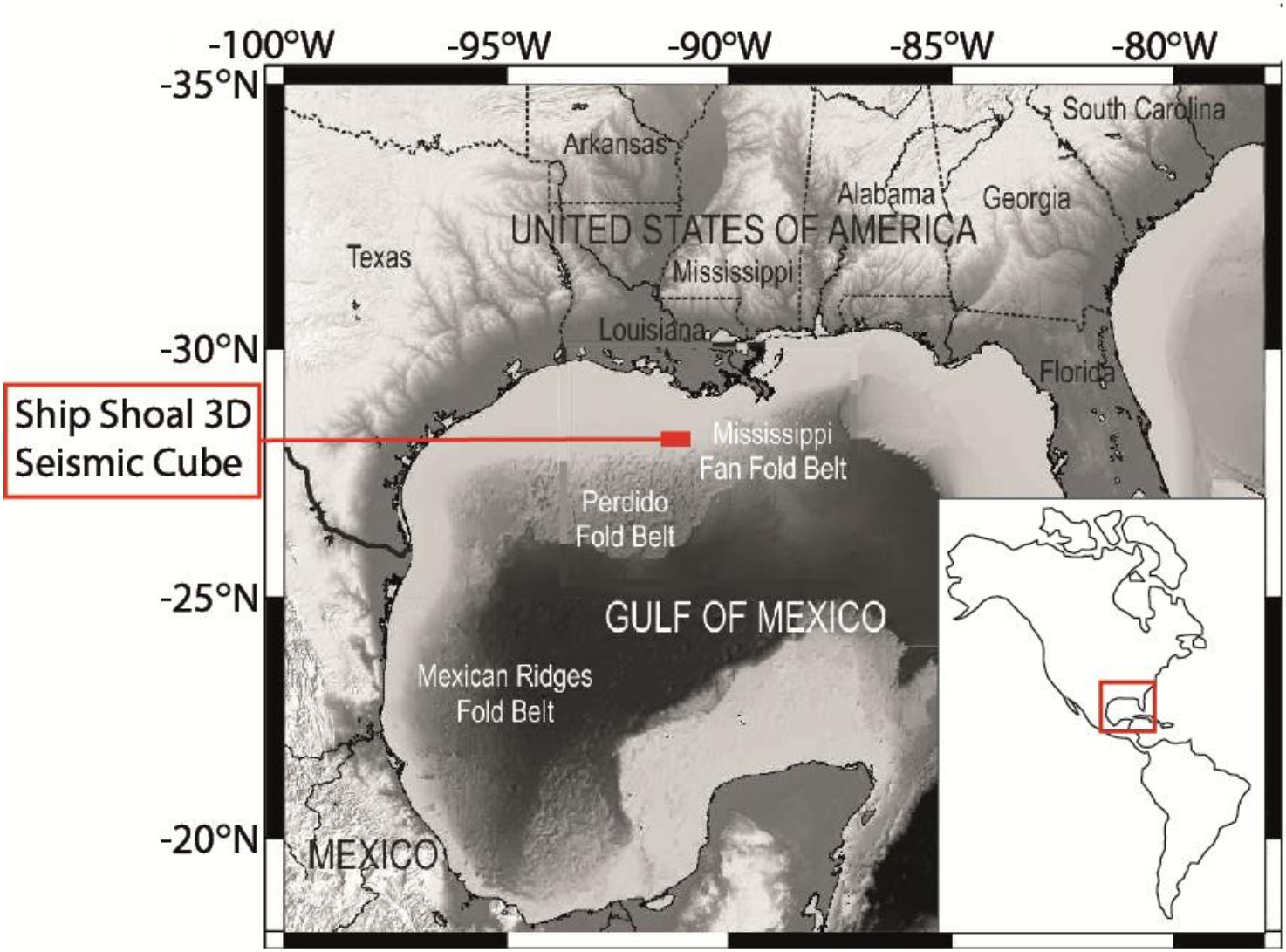

Figure 1: The Gulf of Mexico, south of the United States of America, with the location of the Ship Shoal 3D seismic cube. The seismic cube is situated just north of the Perdido Fold Belt and west of the Mississippi Fan Fold Belt. The Gulf of Mexico basin is considered to be a passive margin (Yassir and Zerwer 1997); and is composed of several upper Jurassic to Pleistocene delta systems that prograded from the north and west (Galloway 1989, Fiduk et al. 1999). The basin is one of the world's most prolific petroleum provinces (adapted from King et al. 2012).

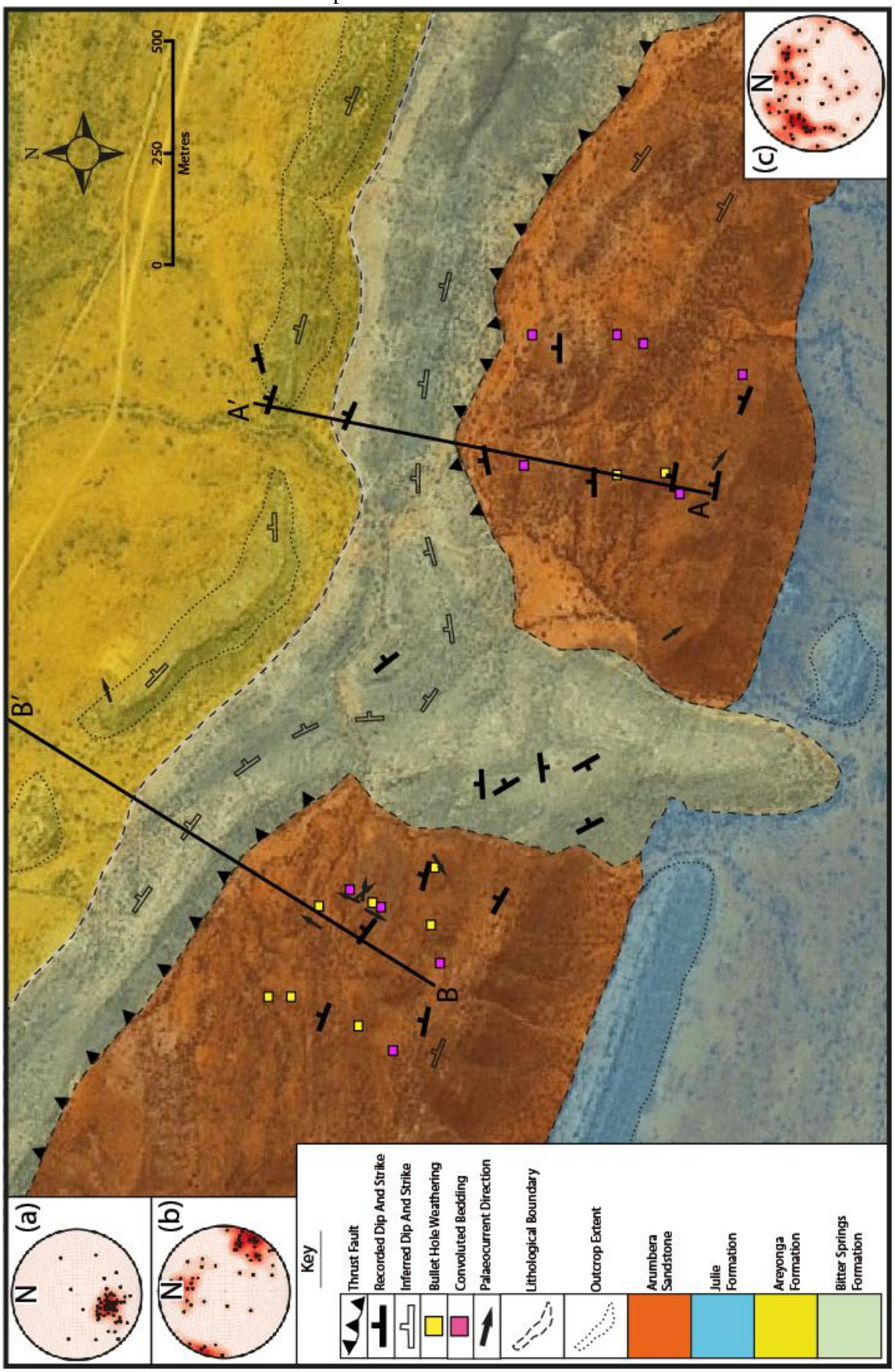

Figure 2: Geological map of the studied salt diapir in the Amadeus Basin, central Australia. The location is approximately 90 kilometres east of Alice Springs. The map includes the lithological units encountered as well as the location of convoluted bedding, bullet hole weathering and palaeocurrent directions calculated from sedimentary structures. Stereonets include (a) poles to bedding for the Arumbera Sandstone, (b) poles to fracture planes for the Arumbera Sandstone on the western flank of the diapir and (c) poles to fracture planes for the Arumbera Sandstone on the eastern flank of the diapir. Cross sections A to A' and B to B' are included in Figure 13.

2. BACKGROUND

2.1 The Gulf of Mexico

The Gulf of Mexico is located south of the United States of America and is one of the world's most prolific petroleum provinces. The Gulf of Mexico basin is considered to be a passive margin (Yassir and Zerwer 1997) and is composed of several upper Jurassic to Pleistocene delta systems that prograded from the north and west (Galloway 1989, Fiduk et al. 1999). Beneath the deltaic sediments, the Louann Salt acts as a regional detachment (King et al. 2012, Wu et al. 1990) and is a source for extensive diapirism (Jackson et al. 1994). Although it is not widespread, allochthonous and shallow salt sheets also lay stratigraphically above the Louann Salt (Rowan and Vendeville 2006). The formation of these salt sheets and tongues was due to dominant down-slope spreading and over-thrusting of salt within unconsolidated sediment during the Mid-Miocene to Plio-Pleistocene, a consequence of continued rapid sediment accumulation (Wu et al. 1990). As the Louann Salt acts as a regional detachment, the continuous progradation of sediment has caused the formation of a DDWFTB. Gravitational collapse at the delta top causes extensional normal faulting in an extensional stress regime. This is associated with a thrust fault and compression system at the delta toe, as described by many authors (e.g. King et al. 2009, Rowan 1997, Dooley et al. 2007, Morley 2009, McClay et al. 2003).

The geological history of the Gulf of Mexico is dominated by both eustatic variations and subsidence evolution (Galloway et al. 2000, Wilhelm and Ewing 1972). The middle Pennsylvanian Ouachita orogeny in the southern United States represents the

consolidation of the Gulf of Mexico's Palaeozoic basement (Wilhelm and Ewing 1972). Post Ouachita orogenic strata (Pennsylvanian), resting unconformably on the Ouachita fold belt, have been encountered in coastal regions of Louisiana and Texas (Wilhelm and Ewing 1972). This post-orogenic deposition is assumed to have reached the Gulf of Mexico. Following this, the Jurassic Louann Salt was then deposited and is the result of a subsidence-driven marine transgression that spread over Mexico and the southern United States (including the East Texas Basin) (Wilhelm and Ewing 1972, Jackson and Seni 1983). The original thickness of the Louann Salt is unknown due to extensive salt flows and diapirism, but it is estimated to have been at least 1,500 m thick (Jackson and Seni 1983). Post-salt stratigraphy can be divided into four major sequences that represent the evolution of the Gulf of Mexico (Rowan 1997). The Upper Jurassic Challenger Carbonates were deposited in a shallow marine environment. This then transitions to a deeper marine environment represented by the deposition of the Cretaceous Campeche chalk and shales (Rowan 1997). Next, the Mexican Ridges sequence represents deltaic sands that were deposited near the coast throughout most of the Cenozoic. These were associated with carbonates and turbidites which bypassed the deltaics and were deposited in the deepwater (Rowan 1997). Deposited in the Plio-Pleistocene, the Mississippi Fan is the final sequence of deltaic sands. This unit is also associated with deepwater turbidites and is made up of several delta lobes (Rowan 1997).

2.2 The Amadeus Basin

The Amadeus Basin is a broad intracratonic basin in central Australia that is made up of predominantly shallow-water sediments deposited during the Neoproterozoic and early

Palaeozoic (Lindsay 1987b). The basin lies at the centre of the Australian continent, with Alice Springs, Northern Territory, situated on its northern margin. Along its longest axis, the Amadeus Basin extends approximately 800 km east to west and is bordered to the north and south by large-scale thrust belts. Although this is the case, the centre of the basin has remained relatively undeformed (Kennedy 1993). The Amadeus Basin is composed of a succession of shallow water sediments that lay unconformably on the, much older (1000 - 1800 Ma), Arunta Inlier (Lindsay 1987b, Collins and Shaw 1994). The oldest unit is the Proterozoic fluvial to shallow marine Heavitree Quartzite. The age of this unit is thought to be no older than 897 Ma, a value obtained using Rb-Sr dating of the Stuart Dyke Swarm, which lays unconformably beneath the Heavitree Quartzite (Black et al. 1980). The Bitter Springs Formation rests conformably on top of the Heavitree Quartzite, it is therefore likely that it was deposited at approximately 800 to 700 Ma (Lindsay 1987b). The Bitter Springs Formation is composed of a combination of evaporites (salt) and carbonates. This unit represents an unsubstantiated connection to the ocean with often hypersaline basin waters (Lindsay 1987b). After the Bitter Springs Formation, sedimentation of shallow marine sands, silts and carbonates continued through to the Cenozoic, forming an array of various formations and sub-members.

The Amadeus Basin has undergone structural deformation due to two orogenic events, represented by the large scale thrust belts to the north and south of the basin. Firstly, the Petermann Orogeny involved northward, early Cambrian aged, thrusting of the Musgrave Inlier over the southern margin of the basin (Sandiford and Hand 1998). Secondly, the Alice Springs Orogeny involved southward, Carboniferous aged,

thrusting of the Arunta Inlier over the northern margin of the Amadeus Basin (Sandiford and Hand 1998). The Alice Springs Orogeny has resulted in uplift of the north-eastern flank of the basin, providing suitable outcrop for studying sedimentary and salt-related structures.

2.3 Salt Diapirs

2.3.1 CLASSIFICATION

A descriptive summary of the various types of salt diapirs is given by Jackson et al. (1994). This study is presented as a guide for geophysicists and emphasises the difficulty of imaging the base of salt sheets and subsalt structures targeted for exploration. Using real examples of seismic images and detailed figures, the authors explain the three modes of salt diapirism. 1) A *reactive diapir* pierces the overburden, filling space created by the movement of overburden fault blocks. Reactive diapirs typically form during extensional faulting (Jackson et al. 1994). However, reactive diapirs can also form as a result of thrust movement (e.g. Kent 1979). 2) An *active* diapir pierces by lifting and shoving aside its sedimentary roof (Jackson et al. 1994). 3) A diapir becomes *passive* once it emerges at the surface. As it grows taller, a growing passive diapir remains at or near the sediment surface while its base sinks along with the adjoining sediments (the process of *downbuilding*) (Jackson et al. 1994).

Reactive, active and passive diapirs have their own distinct characteristics associated with deformation style. Nokes (2011) used 3D seismic data from the Gulf of Mexico to build 2D finite numerical models from representative sections of each type of salt diapir. During the interpretation process of this study, the author describes physical

observations related to each type. From Nokes (2011), *reactive diapirs* typically have a triangular shape; their size is related to and controlled by the amount of regional extension and sediments bent upwards approaching the salt diapir are due to subsidence along the flanks of the diapir (Nokes 2011). *Active diapirs* have discrete, local extensional faults visible on seismic profiles and their sedimentary roof is thinned by extensional faulting, with fault blocks dispersed outwards. Strata displaced by slumping is accumulated and re-deposited next to the diapir (Nokes 2011). *Passive diapirs* typically evolve to a steep sided, flat crested structure and are surrounded by strata that show little faulting and thickness change. Passive diapirs can revert back to active form when sedimentation increases (Nokes 2011). In this study, the preceding characteristics were used to assist with the interpretation of salt diapirs in the Gulf of Mexico using the Ship Shoal 3D seismic cube.

2.3.2 SALT PROPERTIES

Salt is mechanically weak and over geological time will act as a Newtonian fluid (Hudec and Jackson 2007); where a linear relationship exists between stress and strain. Due to its geomechanical properties, salt is incompressible, and therefore, when buried at depth below overburden of a greater density, salt becomes buoyant and gravitationally unstable (Jackson and Talbot 1986). This property allows salt to act as a regional detachment and is fundamental to the formation of salt diapirs.

2.3.3 SEISMIC STUDIES

A study completed by Davison et al. (2000) used seismic data to interpret the structural evolution of Central Graben salt diapirs in the North Sea. This study found that the

diapirs grew by progressive downbuilding for most of their history. More recently, King et al. (2012) used numerical 3D modelling to better understand the geomechanical aspects controlling the observed local stress deflections around salt diapirs (for the purpose of the model, all diapirs were assumed to be passive). This was completed using the 3D Ship Shoal seismic cube and focused on the displacements, strain and stresses around the top Louann Salt (Jurassic evaporites, Gulf of Mexico). It was found that when an extensional stress regime was applied to the model, net normal displacement occurred with displacement vectors perpendicular to the flanks of salt diapirs (King et al. 2012).

2.3.4 PREVIOUS FIELD WORK

Similar studies have been made using outcrop observations of salt structures. This has its benefits as the observations that can be made using seismic data are limited by the horizontal and vertical resolutions of the data. Provided there is good quality outcrop, field observations can be made at centimetre scale, providing a finer qualitative description of the structural and sedimentary characteristics associated with salt diapirs.

Outcrop analysis of deltaic sediments adjacent to salt diapirs was completed by Alsop et al. (2000) at Cape Breton Island, Nova Scotia. The authors described “drag zones”, which were identified as highly strained regions developed adjacent to the flanks of salt diapirs, and are produced when the sedimentary overburden is folded or rotated into steeply dipping attitudes sub-parallel to the diapiric walls (Figure 3). Due to these steep dips, seismic interpretation of drag zones is problematic (Alsop et al. 2000). Thus, outcrop observations are invaluable. One of the most significant conclusions of this

study was the observation of minor extensional fractures within the drag zones. These fractures typically formed conjugate sets either parallel or orthogonal to the diapiric margin. At greater distances from the diapir however, where strain rates are lower, deformation occurs by creep processes resulting in increased bedding dips, but no enhanced fracturing (Alsop et al. 2000).

Earlier outcrop analysis was completed by Kennedy (1993) in the Amadeus Basin, central Australia. Rather than focussing on structural deformation, this study looked closely at the thickening of sediments adjacent to a salt diapir, specifically the late Proterozoic salt influenced deposition of the Undoolya Sequence. This 710 m thick sequence is interpreted to have been deposited syn-depositionally (syn-diapiric) in a peripheral "sink" adjacent to the diapiric Benstead Creek Structure (Kennedy 1993). Field observations included the identification of a sequence of fine-grained turbidites adjacent to the Benstead Creek Structure. The observation suggested a rapid deepening of the adjacent basin (Kennedy 1993).

2.3.5 PHYSICAL MODELS

Previous models have been used specifically to simulate the physical conditions of diapir evolution. Rowan and Vendeville (2006) used differential loading of sediment to examine the deformation styles of mini-basins surrounded by salt ridges. Diapir growth was triggered by downbuilding of the mini-basins, after which the model was shortened to simulate a compressive regime. This led to the diapirs localising the contractional strain and simple translation of the mini-basins, causing surface extrusion of the salt diapirs. This model was compared against two natural examples. Firstly, the northern

Gulf of Mexico, where up dip gravity spreading caused distal shortening during the Miocene (Rowan and Vendeville 2006). Secondly, in the Flinders Ranges, South Australia, where Neoproterozoic diapirism occurred prior to the Cambro-Ordivician Delamerian Orogeny (Rowan and Vendeville 2006).

Ge et al. (1997) looked more closely at the importance of progradation as a trigger for salt tectonics and formation of allochthonous sheets. In this study, deposition of prograding sediments occurring above an initially flat layer of salt was simulated. Primarily the gravitational loading of the sediments squeezed the salt basinward, forming a relict salt pillow and horizontal salt weld attaching the sediments to the basement (Ge et al. 1997). A second test involved the same sedimentation and salt layer but the basement was uneven, with landward dipping subsalt normal faults. In this test one of the fault scarps acted as a buttress, forming a large salt anticline which deformed the sediments around it (Ge et al. 1997).

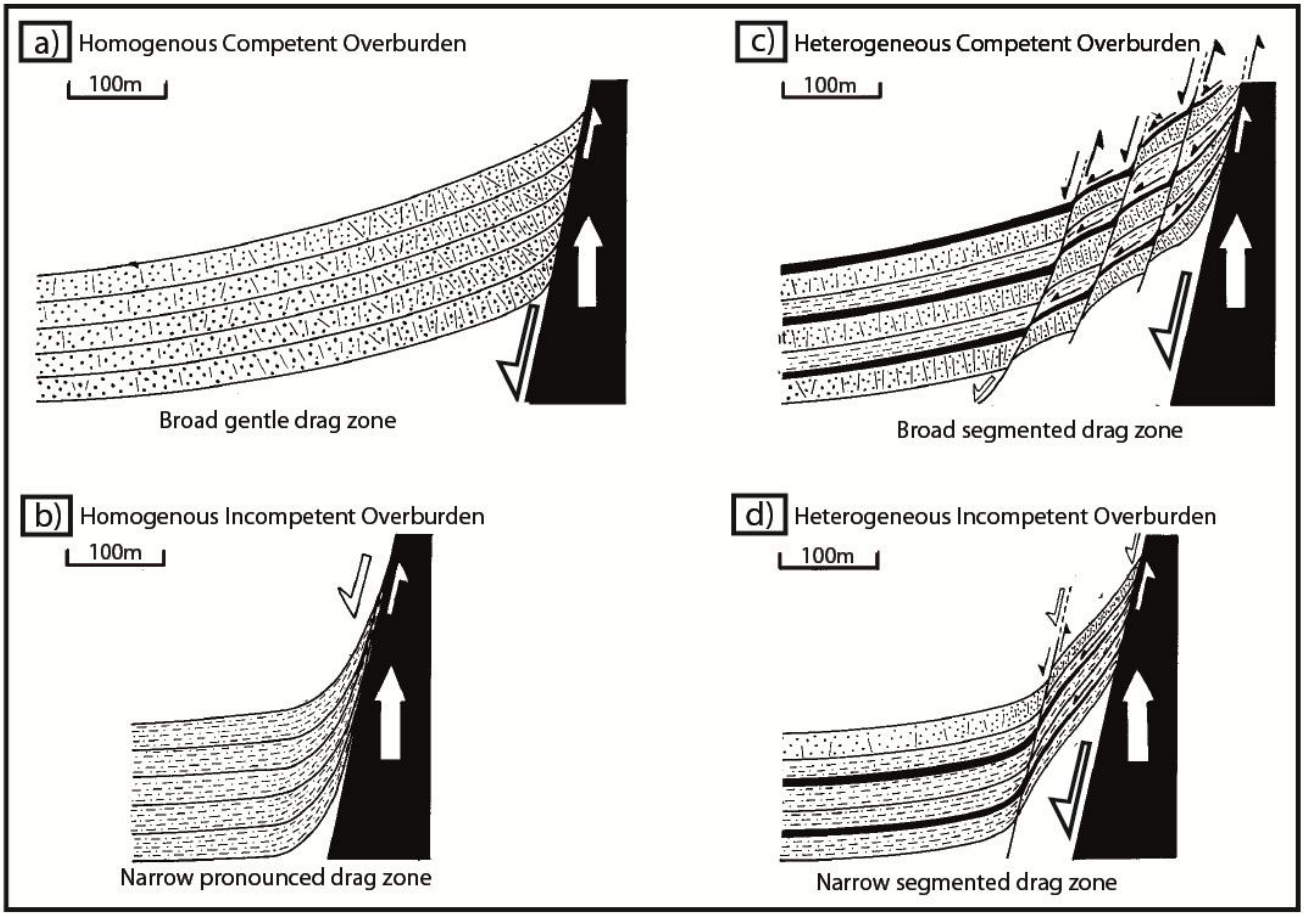

Figure 3: A schematic diagram of sediment drag zones on the flanks of salt diapirs with varying types of deformation related to the competence and heterogeneity of overburden. (a) Homogenous, competent overburden forms a broad, gentle drag zone with fracture density decreasing away from the diapir margin. (b) Homogenous, incompetent overburden forms a narrow, pronounced drag zone with little fracturing and prominent downbuilding. (c) Heterogeneous, competent overburden forms a broad, segmented drag zone with late extensional fractures, similar to the deformation observed in Figure 5. (d) Heterogeneous, incompetent overburden forms a narrow, segmented drag zone with an abrupt increase in bedding dip due to gravitational collapse (adapted from Alsop et al. 2000).

3. SEISMIC INTERPRETATION IN THE GULF OF MEXICO

3.1 Method of Seismic Interpretation

Seismic data has been a preferred option for the study of subsurface salt structures for many authors (for example Wu et al. 1990, Morley et al. 1996, Davison et al. 2000 and Treviño et al. 2008). In this study, the Ship Shoal 3D seismic cube from the Gulf of Mexico was used to interpret the in-situ stress orientation within close proximity to

subsurface salt diapirs. A top salt horizon layer was initially interpreted throughout the seismic cube. After this was complete, each salt diapir that was to be included in the study was interpreted for the top pre-diapiric sediment horizon, in order to gain an understanding of the evolution of each diapir. Structural interpretation then involved the identification of faults and fractures on the flanks of the diapirs. The subsequent orientation of σ_H was then implied from this evidence.

3.2 Gulf of Mexico Observations

The spatial arrangement of salt diapirs is shown using an appropriate depth time slice of the 3D seismic cube (Figure 4). A total of 5 salt diapirs are interpreted from the seismic data. Although this is the case, due to the varying seismic reflection quality only 2 were analysed. These salt diapirs are denoted as D1 and D2 (Figure 4). For each of the 2 diapirs, the top salt and top pre-diapiric sediment horizons are interpreted. As well as this, structural analysis of faults and fractures adjacent to both diapirs was completed and is represented by Figures 5 to 8.

Structural deformation characteristics associated with D1 include normal faults proximal to the sediment-diapir interface. The deformation pattern to the west of D1 (Figure 5) is interpreted to be a sediment drag zone, similar to what is described by Alsop et al. (2000) (Figure 3). The north-south vertical section of D1 displays tilted faulted blocks in close proximity to the diapir wall (Figure 6). However, these faults are dipping towards the diapir, rather than away from, suggesting that these collapse structures are a result of salt withdrawal from underneath the deltaic sediment, further contributing to the downbuilding of the adjacent mini-basin.

The east-west section of D2 also includes a section of D1 as the two are in close proximity to each other (Figure 7). Diapir 2 has normal faults interpreted on its western flank and sediment horizons are interpreted to thicken due to syn-depositional fault movement. A single thrust event is interpreted to lie on the western flank of D2 and stratigraphically above the majority of normal faults (Figure 7). The north-south section of D2 (Figure 8) displays much the same characteristics as D1 (Figure 5), in that normal faults are interpreted proximal to the diapir wall and dip away from the diapir. A zone of prograding seismic facies exists within the deltaic sediment (Figure 8c). This zone of layered progradations is well pronounced amongst the otherwise laminar and flat lying layers of deltaic sediment and infers a sediment-flow direction away from the diapir.

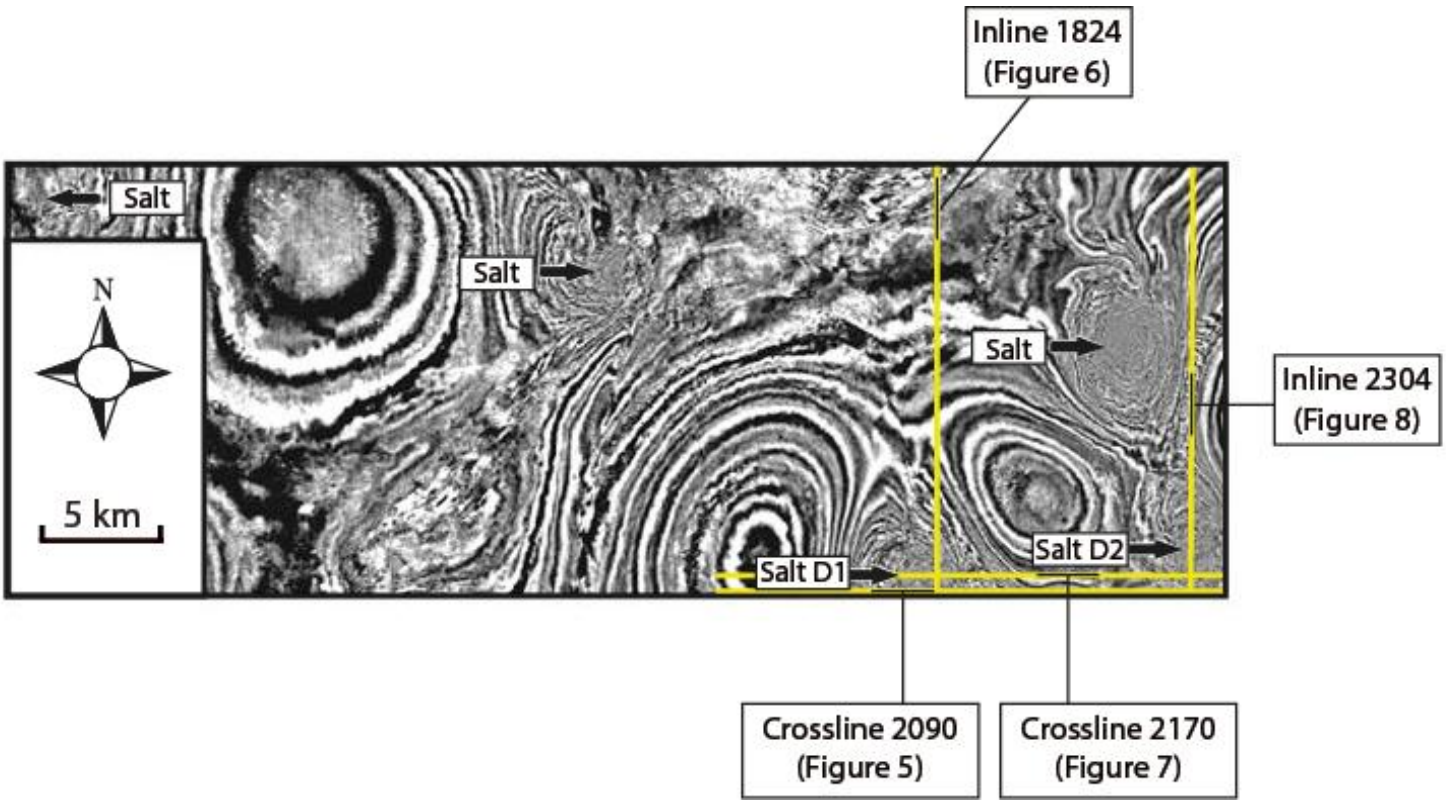

Figure 4: A 1 second time slice of the Ship Shoal 3D seismic cube. Salt diapirs can be seen as zones of chaotic reflections in between distinctively layered minibasins. Yellow lines represent vertical seismic sections used for this study. D1 and D2 denote the two salt diapirs used for interpretation. Other salt diapirs within the 3D volume were discounted due to varying seismic reflection quality (adapted from Nokes 2011).

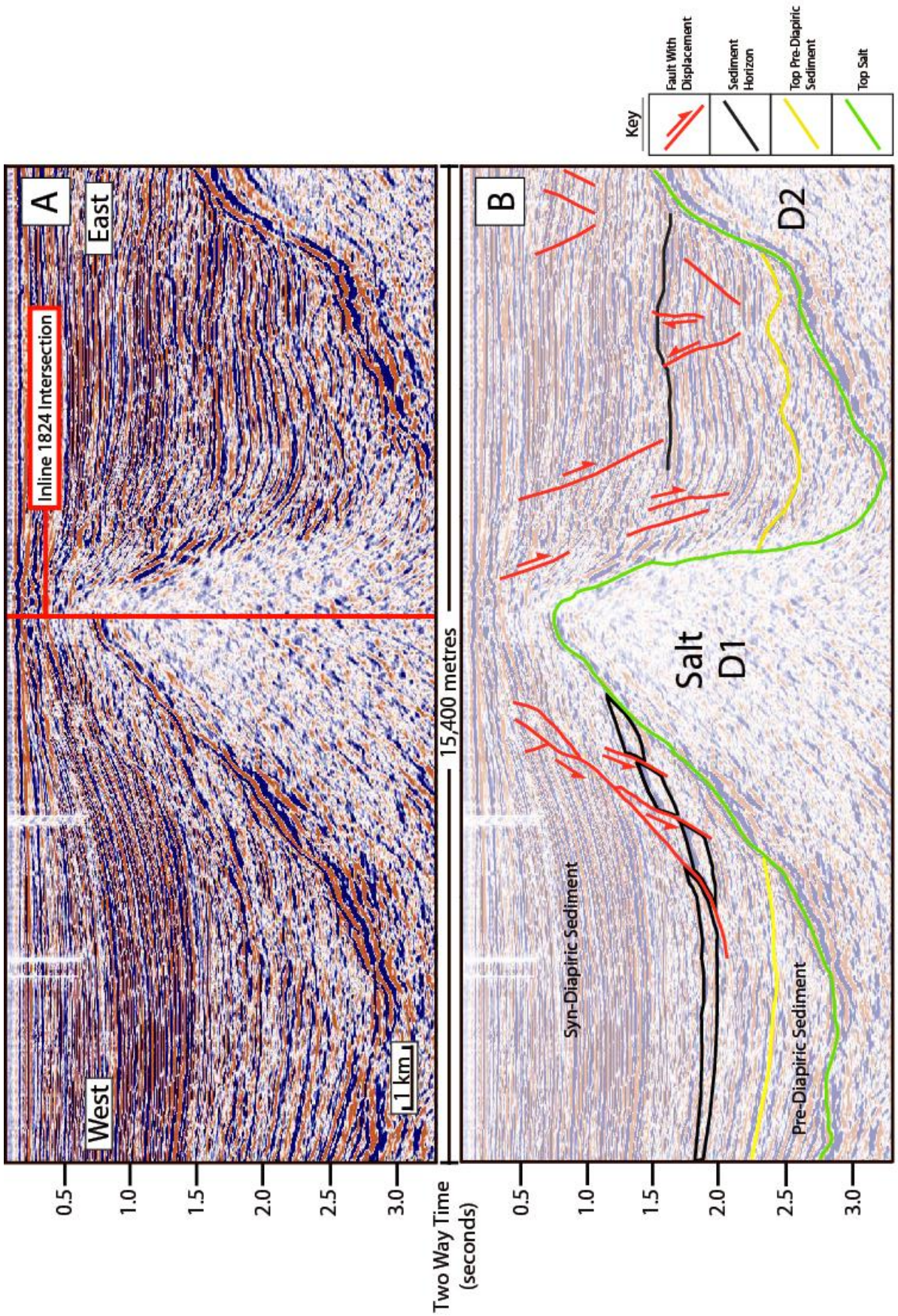

Figure 5: Crossline 2090, an east-west vertical seismic section of D1. A) Vertical section without interpretations. B) Vertical section with an overlay of interpretations. Top salt and top pre-diapiric sediment horizons have been interpreted and plotted. Structural observations include net normal displacement on both the eastern and western flanks of the diapir. Note the array of normal faults on the western flank of the diapir forming a sediment drag zone. This is similar to the model suggested by Alsop et al. (2000). Net normal displacement suggests that the σ_H orientation has been locally deflected from the delta top margin parallel, to become sub-parallel to the salt-sediment interface.

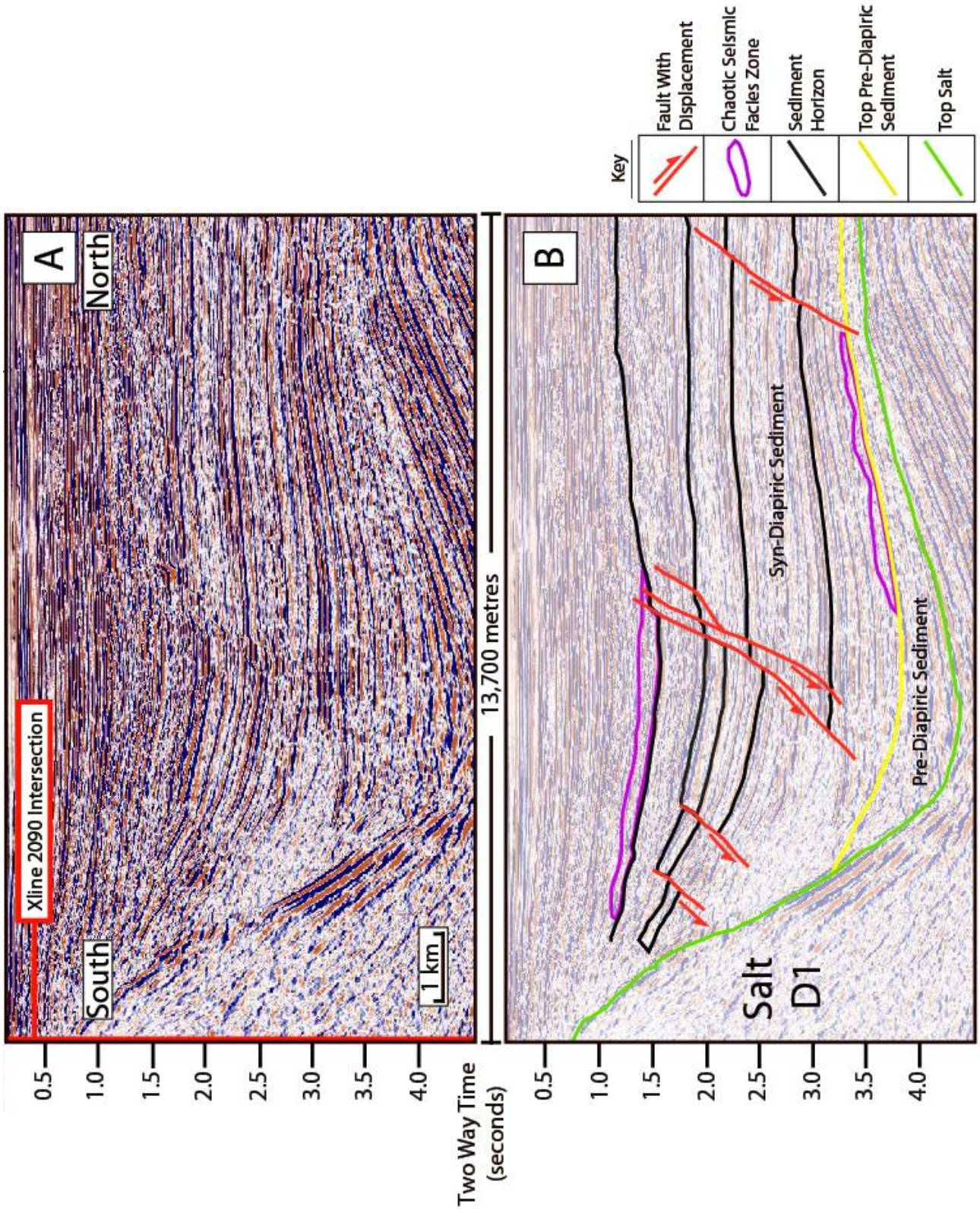

Figure 6: Inline 1824, a north-south vertical seismic section of D1. A) Vertical section without interpretations. B) Vertical section with an overlay of interpretations. Top salt and top pre-diapiric sediment horizons have been interpreted and plotted. Structural observations include net normal displacement on the northern flank of the diapir. Normal faults are dipping towards the diapir, rather than away from, suggesting that these faults are attributed to salt withdrawal from beneath the deltaic sediment. This salt withdrawal is associated with downbuilding and assists with deposition in to the minibasin by creating accommodation space. Zones of chaotic seismic facies are due to reflections from heterogeneous, high energy sediment flows from the diapir during periods of active movement.

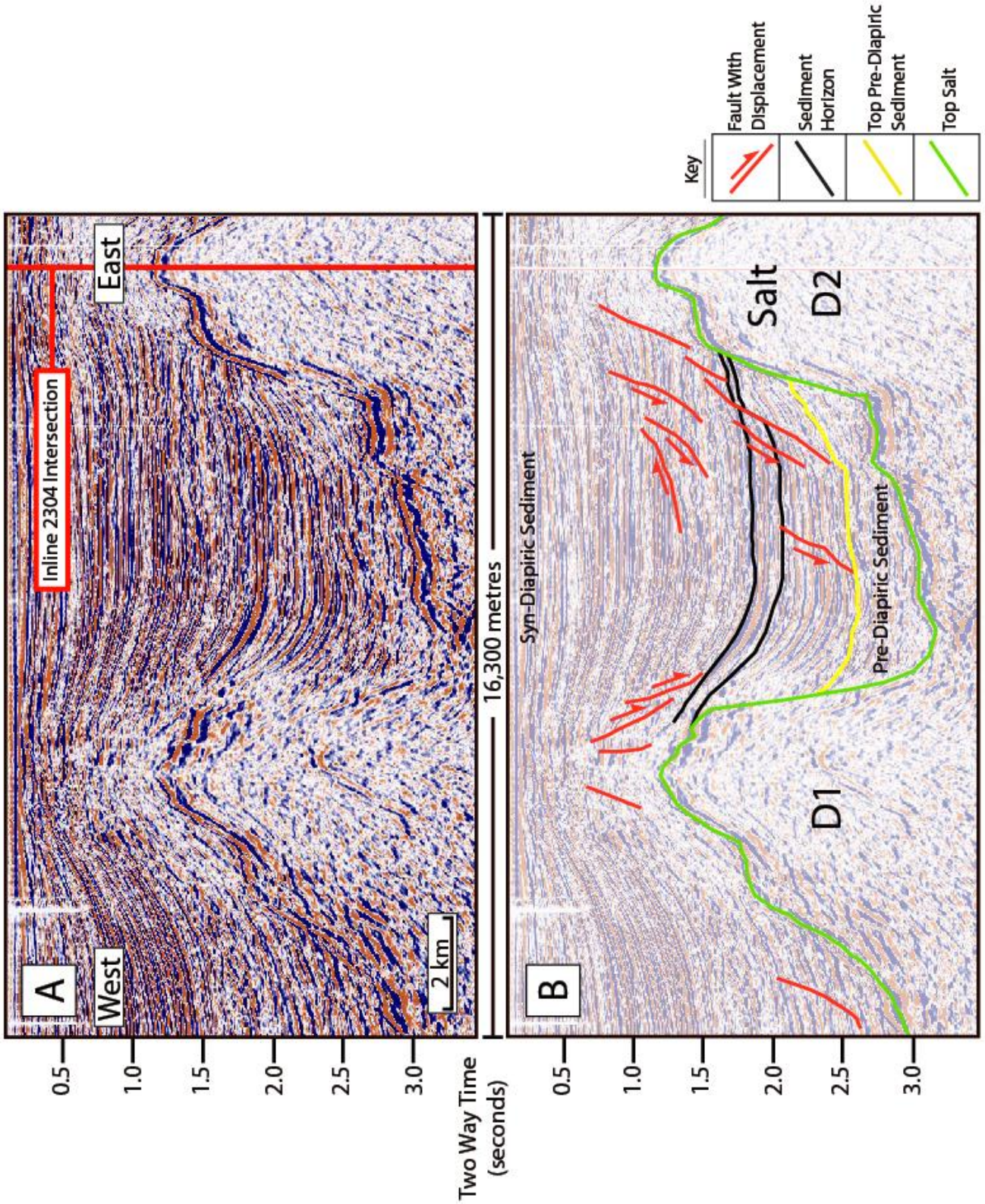

Figure 7: Crossline 2170, an east-west vertical seismic section of D1 and D2. A) Vertical section without interpretations. B) Vertical section with an overlay of interpretations. Top salt and top pre-diapiric sediment horizons have been interpreted and plotted. Structural observations include normal faults along the western flank of D2 and the eastern flank of D1. As with Figure 5, this observation suggests that σ_H is deflected to become sub-parallel to the salt sediment interface. Net normal displacement on the flanks of both diapirs is associated with progressive downbuilding of the minibasin. Out of the 7 displacements interpreted, 1 shows a reverse sense of movement. This suggests that there is a small degree of variability with in-situ stress, particularly when two salt diapirs are in close vicinity.

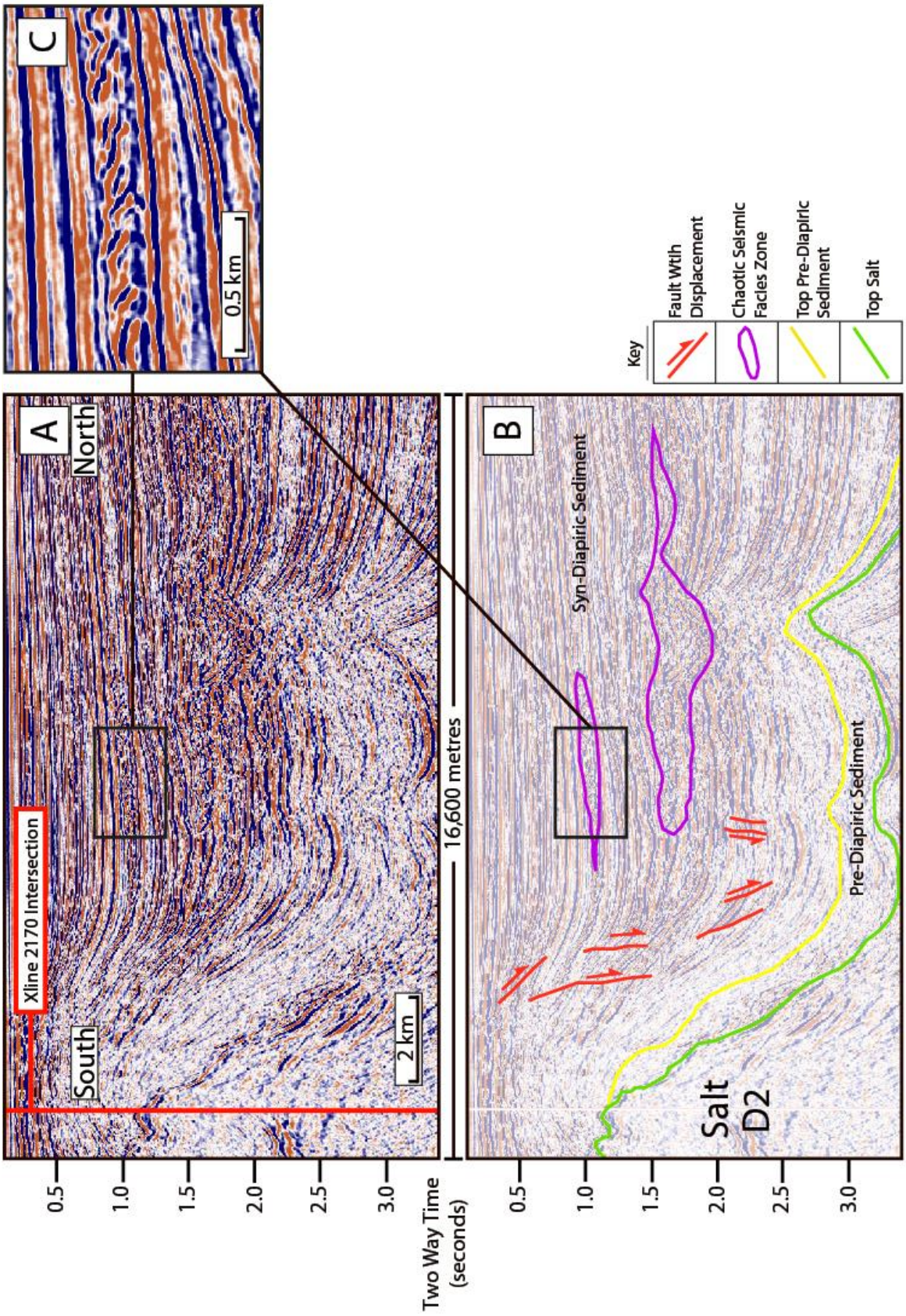

Figure 8: Inline 2304, a north-south vertical seismic section of D2. A) Vertical section without interpretations. B) Vertical section with an overlay of interpretations. Top salt and top pre-diapiric sediment horizons have been interpreted and plotted. Structural interpretations include net normal displacement on the northern flank of the diapir, suggesting that σ_H is deflected sub-parallel to the salt-sediment interface. C) A close up view of a zone of short, prograding reflections. This zone is well pronounced amoung the otherwise laminar and flat lying layers of deltaic sediment and infers a sediment-flow direction away from the diapir during active diapir movement.

4. AMADEUS BASIN FIELD WORK

4.1 Field Methods

In the study area it is interpreted that the Bitter Springs formation has intruded the Arumbera Sandstone and hence has acted as a salt diapir (Figure 2). Field observations and data collection included both sedimentary and structural characteristics. These were recorded along a series of 6 transects (Appendix C). This included 2 north-south transects on both the western and eastern flanks of the diapir, 1 north-south transect within the diapir and 1 east-west transect along the southern ridge top. The tabulated sedimentary and structural observations of the lithological units were used to study the palaeostress orientation during deformation. Emphasis for this was placed on conjugate pairs that possess the idealistic angles between fracture planes of 60^{o} and 120^{o} (Figure 9). Pairs of fractures that dissect each other with angles that differ more than 15^{o} outside of the ideal angular relationship were discounted. Those that have angular relationships within 15^{o} of this ideal were included for palaeostress analysis.

4.2 Amadeus Basin Field Observations and Data

4.2.1 STRATIGRAPHY OF THE STUDY AREA

Three geological units were encountered in the Amadeus Basin field area, the Late Proterozoic Bitter Springs Formation and Areyonga Formation and the Late Proterozoic to early Cambrian Arumbera Sandstone. All three units differ with their lithological characteristics and have undergone various levels of structural deformation. A detailed geological map of the area is displayed by Figure 2, with stereonets from field data in Figure 10.

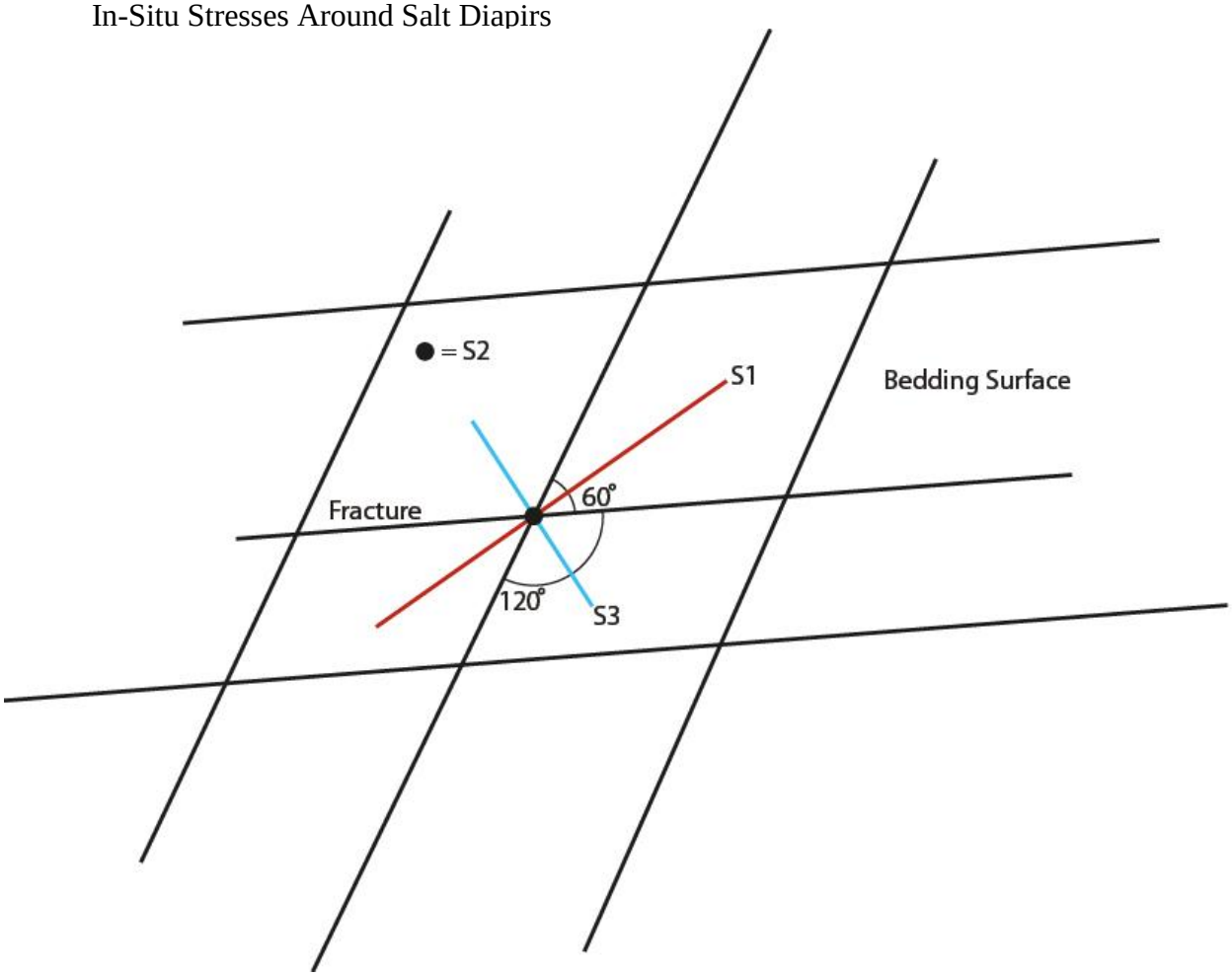

Figure 9: Schematic drawing of a field example of conjugate fractures in the Arumbera Sandstone. Palaeostress orientation can be deduced from the ideal angular relationship between conjugate pairs of 60° and 120°. The maximum principal stress orientation (S1 for σ_1) lies in the middle of the acute angle between conjugate pairs whilst the minimum principal stress orientation (S3 for σ_3) lies in the middle of the obtuse angle. The medium principal stress orientation (S2 for σ_2) is defined as the line of intersection between the two fracture planes. Palaeostress analysis of the Arumbera Sandstone was completed using field measurements of conjugate fractures that possessed the idealistic angular relationship to within 15°.

The Bitter Springs Formation in the field area is a very fine grained, yellow-white to brown dolomite with fine 0.5 cm laminations of dark heavy mineral layers. Occasional centimetre-scale cross beds were encountered, but most of the outcrop displayed fine laminations, indicative of a low energy depositional environment. Structurally, the Bitter Springs Formation had a dominant bedding dip towards the north-northeast. However, within the diapir the bedding orientation became dramatically inconsistent with high levels of brecciation and complex, tightly bounded and randomly orientated folds. In some cases, small fragments of preserved bedding were found amongst an

otherwise brecciated and highly-deformed dolomite matrix (Figure 11). This resulted in bedding planes that were difficult to observe and measure, allowing only few reliable readings of dip and dip direction to be taken from within the diapir.

Laying conformably on top of the Bitter Springs Formation, the Areyonga Formation consisted of a yellow to light red, coarse grained, well-sorted sandstone. Occasional zones of poorly-sorted, grain-supported conglomerate are present, which commonly fined up over approximately 15 centimetres to medium- to coarse-grained sand. The conglomerate layers consisted of subrounded quartz clasts ranging from a few millimetres in diameter to 1.5 cm pebbles. The majority of the unit is quartz rich and mineralogically mature.

The youngest unit is the Late Proterozoic to early Cambrian Arumbera Sandstone. This is a very fine- to medium-grained, dark red to brown, sandstone. Occasional dune scale crossbeds were observed ranging from 3 cm to 50 cm in thickness. The unit is texturally homogenous and uninterrupted, although, in some areas 1 – 3 metre thick dolomite interbeds were observed. Other sedimentary structures included complex convoluted bedding (Figure 12) and bullet hole weathering, potentially forming from the erosion of small concretions. Palaeocurrent directions from dune scale cross beds and ripple crests observed in the Arumbera Sandstone display a large degree of variation with both geographic and stratigraphic positions (Figure 2).

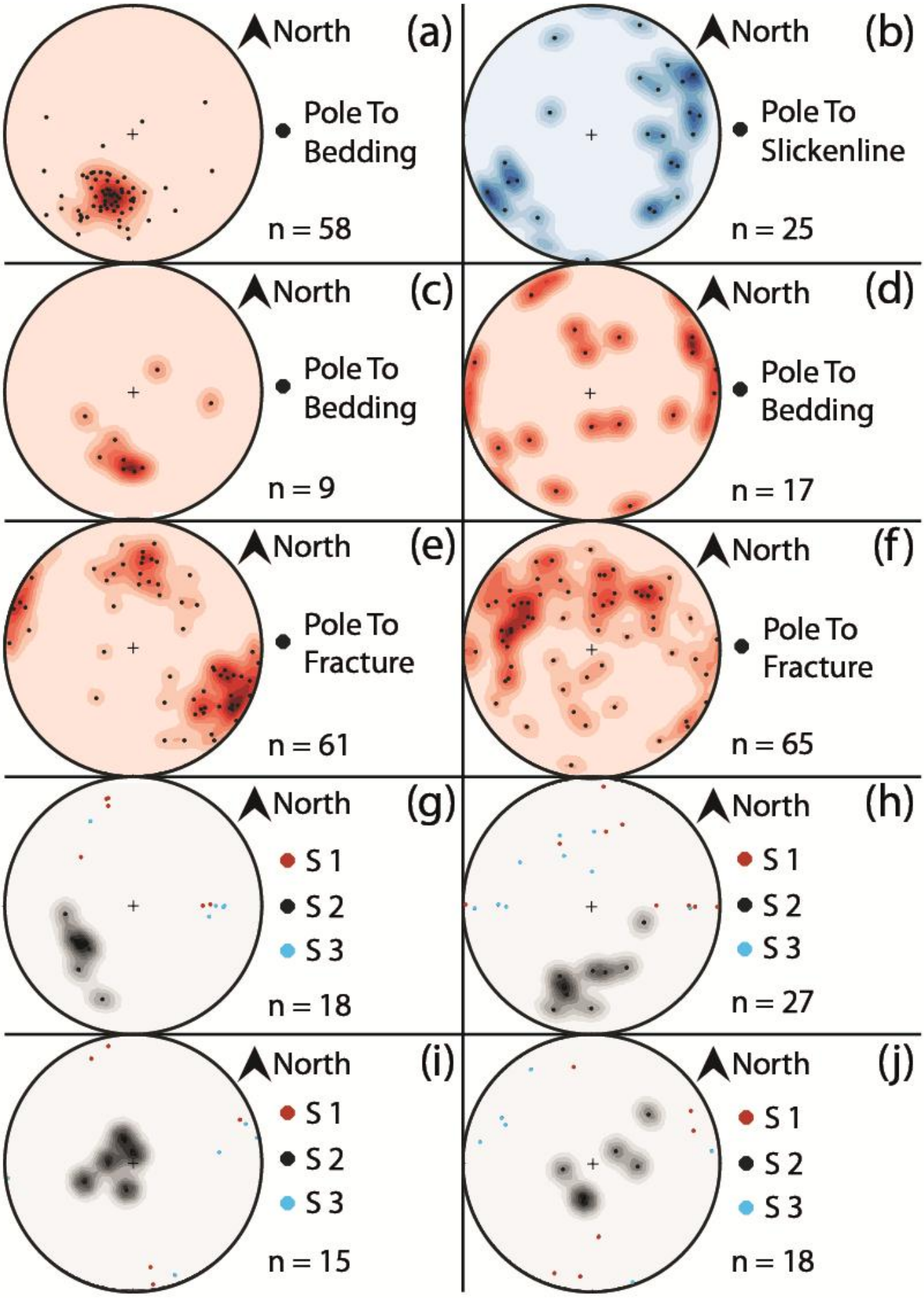
North
(a)
Pole To Bedding
n = 58
North
(b)
Pole To Slickenline
n = 25
North
(c)
Pole To Bedding
n = 9
North
(d)
Pole To Bedding
n = 17
North
(e)
Pole To Fracture
n = 61
North
(f)
Pole To Fracture
n = 65
North
(g)
S 1
S 2
S 3
n = 18
North
(h)
S 1
S 2
S 3
n = 27
North
(i)
S 1
S 2
S 3
n = 15
North
(j)
S 1
S 2
S 3
n = 18

Figure 10: Structural field data displayed stereographically. (a) Poles to bedding for the Arumbera Sandstone with red contours. This demonstrates that the structural trend of the Arumbera Sandstone dips towards the north-northeast. (b) Poles to slickenlines in the Arumbera Sandstone with blue contours. The stereonet suggests a northeast-southwest trend of strike-slip fracture movement. (c) Poles to bedding for the Bitter Springs Formation outside of the diapir with red contours, displaying a structural trend dipping towards the north – similar to the Arumbera Sandstone. (d) Poles to bedding for the Bitter Springs Formation inside the diapir with red contours. The poles to bedding are randomly dispersed across the stereonet due to the highly deformed structural nature of the Bitter Springs Formation within the diapir. (e) Poles to fractures in the Arumbera Sandstone on the western flank of the diapir, with red contours. Two major clusters of fracture orientation are present within the field data, primarily suggesting a particular relationship between the two orientations. (f) Poles to fractures in the Arumbera Sandstone on the eastern flank of the diapir, with red contours. The fracture orientations are more randomised compared to the western flank. The structural deformation on the eastern flank of the diapir is more complex and major trends of fracture orientation cannot confidently be identified. (g) Poles to palaeostress orientations, calculated using conjugate pairs, for the Arumbera Sandstone, on the western flank of the diapir, with grey contours for σ_2. The σ_2 orientations cluster within the south-western quadrant of the stereonet. The σ_1 and σ_3 orientations switch between being oriented towards the east and north-northwest. (h) Poles to palaeostress orientations, calculated using conjugate pairs, for the Arumbera Sandstone, on the eastern flank of the diapir, with grey contours for σ_2. The σ_2 orientations cluster towards the south, with orientations for σ_1 and σ_3 spread across the northern half of the stereonet. Compared with (g), less of a trend can be deduced, as is expected since the fracture orientations on the eastern flank of the diapir vary greatly. (i) Poles to palaeostress orientations corrected for bedding dip, calculated using conjugate pairs, for the Arumbera Sandstone, on the western flank of the diapir, with grey contours for σ_2. After the correction for bedding dip, σ_2 orientations remained clustered and migrate towards the centre of the stereonet, suggesting that σ_2 orientations are perpendicular to the bedding plane, leaving σ_1 and σ_3 orientations sub-parallel to the bedding plane. (j) Poles to palaeostress orientations corrected for bedding dip, calculated using conjugate pairs, for the Arumbera Sandstone, on the eastern flank of the diapir, with grey contours for σ_2. After the correction for bedding dip, σ_2 orientations remained clustered and migrate towards the centre of the stereonet (similar to (i)), suggesting that σ_2 orientations are perpendicular to the bedding plane, leaving σ_1 and σ_3 orientations sub-parallel to the bedding plane.

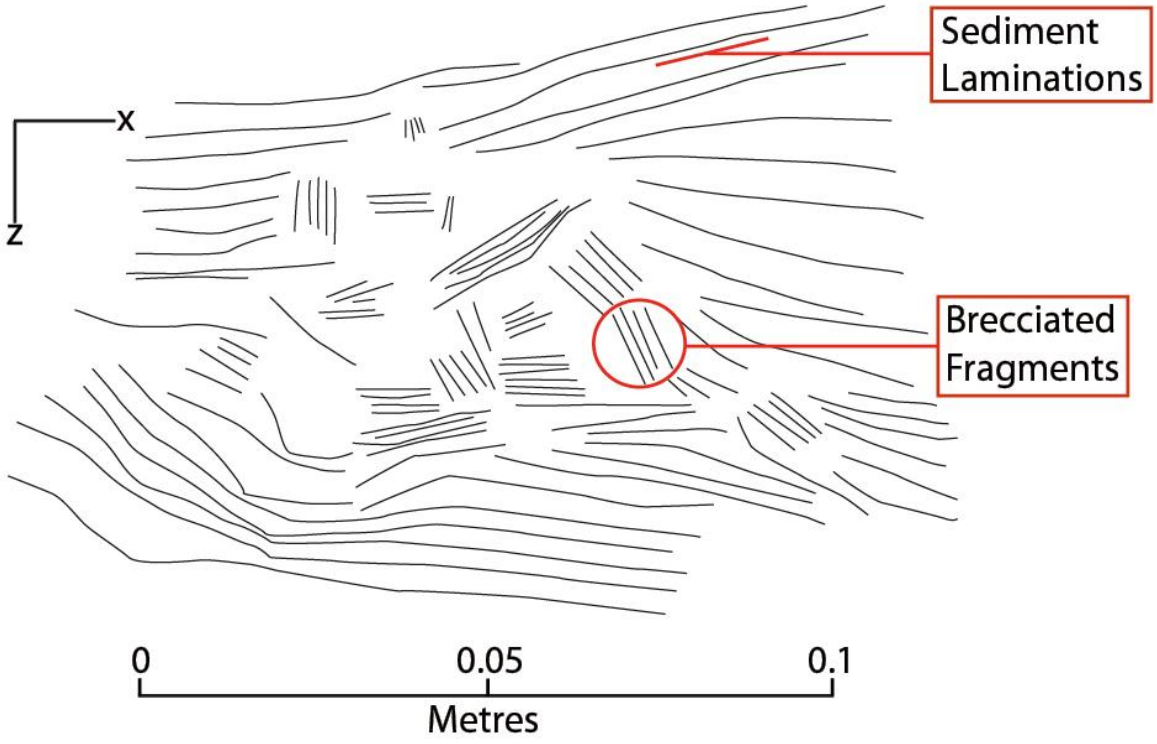

Figure 11: Field sketch of the Bitter Springs Formation within the diapir. It is characteristic in the field area for the Bitter Springs Formation to have 0.5 centimetre laminations with occasional cross beds. However, within the diapir a large degree of brecciation has caused the laminations to become fragmented and randomly orientated. At times, no bedding features can be identified. It is deduced that this deformational characteristic is attributed to active diapir penetration of the Bitter Springs Formation into the Arumbera Sandstone.

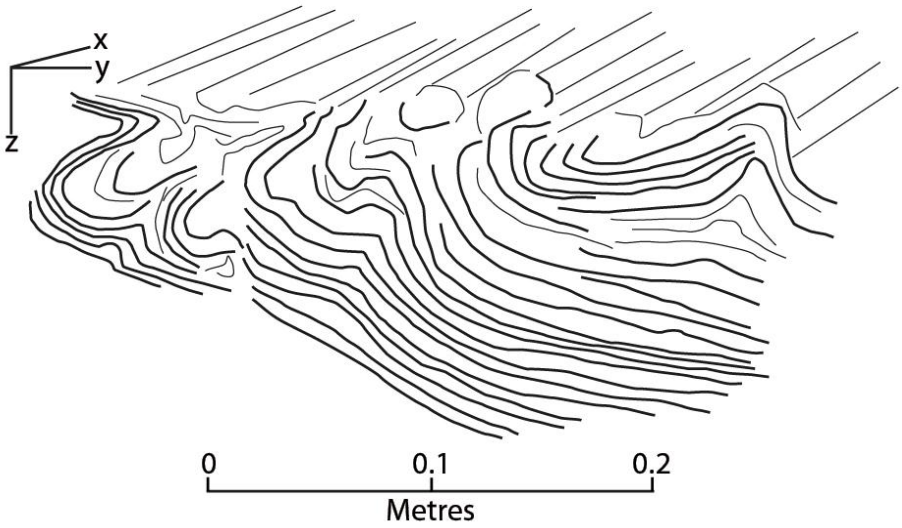

Figure 12: Field sketch of convoluted beds within the Arumbera Sandstone in the field area. Small (0.1 metre) to medium (1 metre) convolutions are apparent in the Arumbera Sandstone across the field area (locations defined in Figure 2). It is known that bedding convolutions can be caused by seismic shaking (Bartsch-Winkler and Schmoll 1984). These convoluted beds are not due to syn-sedimentary active diapir movement, but rather are attributed to tectonic movement from a large bounding normal fault on the northern flank of the Amadeus Basin, as suggested by Lindsay (1987a).

4.2.2 STRUCTURES IDENTIFIED IN THE STUDY AREA

The majority of bedding in the field area dips generally towards north-northeast (Figure 13). Cross bedding and fining up sequences from both the Areyonga Formation and Arumbera Sandstone infer that younging is also towards the north. Structural deformation in the area is dominated by fracture sets that tend to vary in orientation and pervasiveness. The Arumbera Sandstone possessed the majority of fracture planes and the focus for analysis is based on the fracture network of this unit. Out of all the fracture sets measured, a total of 14 displayed the idealistic angular relationship of 120^o and 60^o between conjugate pairs, to within 15^o (Figure 9). These are split into fractures on the west side of the diapir and fractures on the east side (Figures 10e and 10f, respectively). Using structural data, palaeostress orientation was calculated from stereographic projection of conjugate pairs (Figures 10g and 10h). From the data it is evident that σ_2 is clustered relatively tightly on both the western (orientated towards the south-east) and

eastern (orientated towards the south) flanks of the diapir. However, σ_1 and σ_3 tend to vary more considerably. Palaeostress orientation was then corrected for bedding dip, where possible, because the diapir is thought to potentially be a syn-depositional feature. This was projected stereographically (Figures 10i and 10j). When corrected for bedding dip, σ_2 remains as a cluster and migrates towards the centre of the stereonet, implying near vertical orientations that are almost perpendicular to the bedding plane. This migration is the case for both the western and eastern flanks of the diapir; however the cluster remains tighter for the western flank compared to the eastern flank (Figures 10i and 10j).

Slickenlines were observed in the field and measured where possible (Figure 10b). In total, 25 slickenline orientations were collected and out of this data, 22 were interpreted to be due to strike-slip fracture movement after the bedding plane was taken into account. Whether the slickenlines were a result of dextral or sinistral movement could not be determined due to weathered surfaces limiting the outcrop quality. Figure 10b suggests that slickenlines in the field are, as a generalisation, attributed to northeast-southwest directed movement.

Mapping the palaeostress orientations on the geological map is used to assess whether the orientations change in relation to geographic position. Figure 14 displays the palaeostress orientation at each mapping point where an acceptable conjugate pair was found. On both flanks of the diapir it is evident that σ_2 has a consistent trend towards the south-east. The σ_1 and σ_3 orientations are less consistent, as is the case when projected stereographically (Figures 10g and 10h). On the western flank of the diapir, the western most σ_1 orientation trends towards the north, however the σ_1 orientation closest to the

diapir on the western flank trends more sub-parallel to an east-west orientation. This rotation of σ_1 on the western flank of the diapir is the clearest example of an in-situ stress deflection observed in the field.

When corrected for bedding dip, palaeostress orientations placed on the geological map are more clearly defined for σ_1 and σ_3 (Figure 15). As suggested by stereographic projection (Figures 10i and 10j), σ_2 is almost perpendicular to bedding, leaving σ_1 and σ_3 sub-parallel to the bedding plane and becoming highly variable with geographic position.

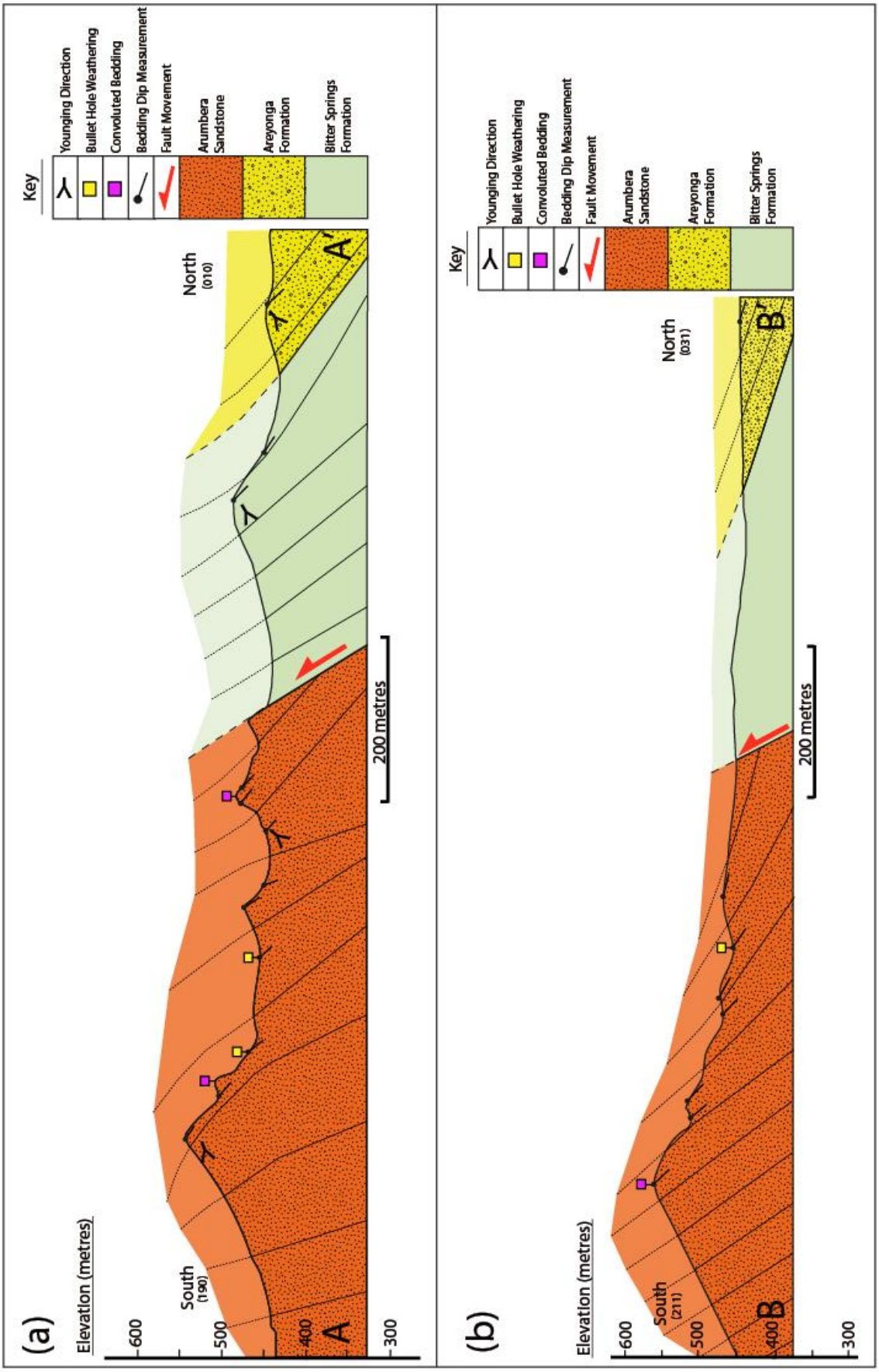

Figure 13: Structural cross sections of the field area. (a) South to north cross section cutting through the Arumbera Sandstone (on the eastern flank of the diapir), the Bitter Springs Formation and the Areyonga Formation. (b) South to north cross section cutting through the Arumbera Sandstone (on the western flank of the diapir), the Bitter Springs Formation and the Areyonga Formation. Cross section locations for (a) and (b) are displayed in Figure 2. Both sections display the structural relationship between lithological units. All three units dip and young towards the north, suggesting that a large thrust exists at the boundary between the Bitter Springs Formation and the Arumbera Sandstone. This is evident as the Late Proterozoic Bitter Springs and Areyonga Formations have been placed on top of the Late Proterozoic to early Cambrian Arumbera Sandstone.

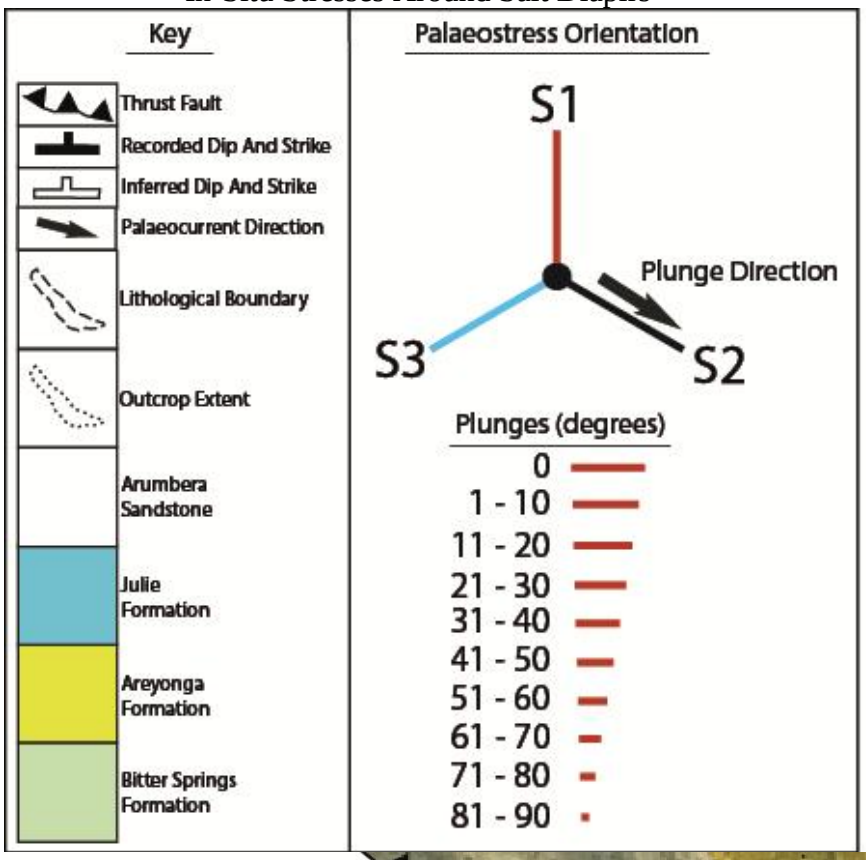

Figure 14: Palaeostress map displaying orientations for σ_1, σ_2 and σ_3 (denoted on the key as S1, S2 and S3). Orientations are calculated from conjugate pairs of fractures in the Arumbera Sandstone at each respective stop on the map. (a) Stereonet displaying palaeostress orientations on the western flank of the diapir. (b) Stereonet displaying palaeostress orientations on the eastern flank of the diapir. (a) and (b) are from Figure 10g and Figure 10h respectively. From this data, σ_2 is consistently plunging towards the south-west on the western flank and towards the south on the eastern flank. The σ_1 and σ_3 orientations tend to vary with geographic position around the diapir. Although this is the case, no particular relationship between palaeostress orientation and the diapir can be deduced.

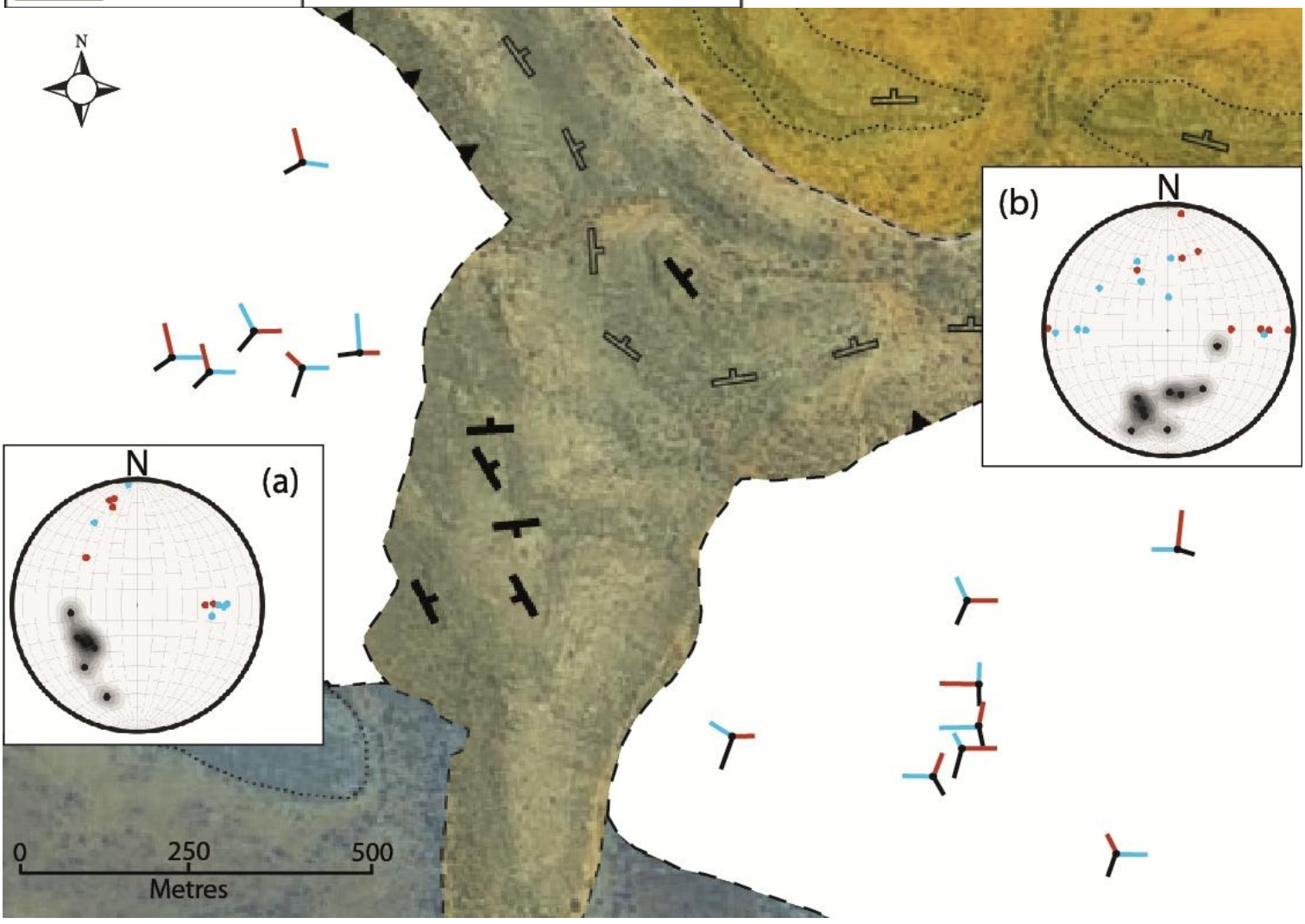

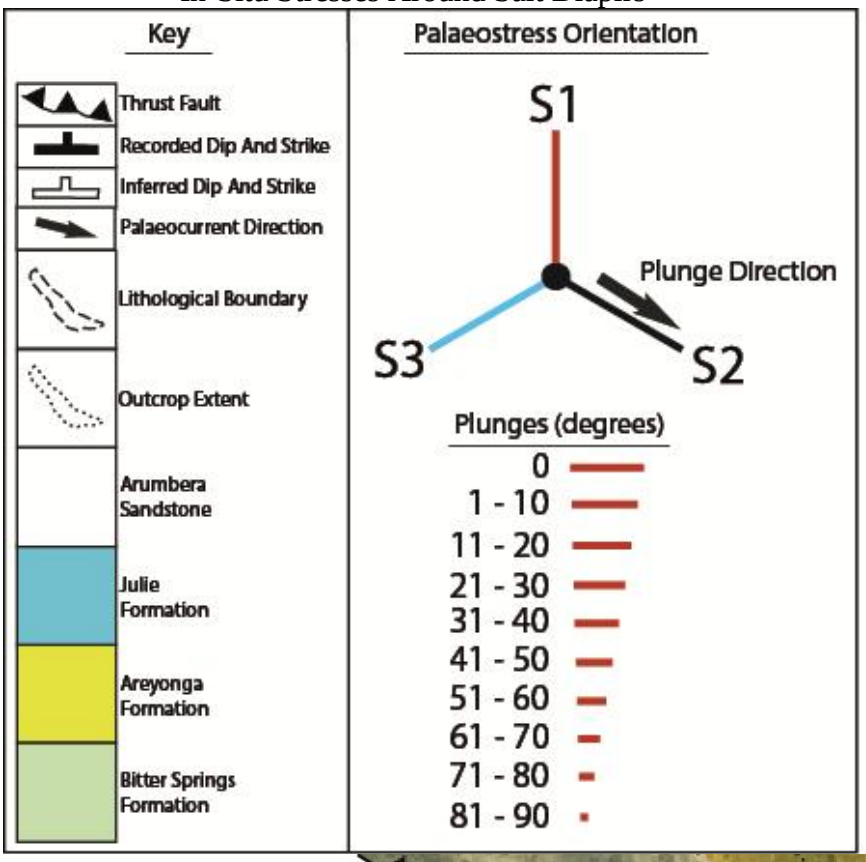

Figure 15: Palaeostress map displaying orientations for σ_1, σ_2 and σ_3 (denoted on the key as S1, S2 and S3), when corrected for bedding dip. Orientations are calculated from conjugate pairs of fractures in the Arumbera Sandstone, and then corrected for bedding dip at each respective stop on the map. (a) Stereonet displaying palaeostress orientations on the western flank of the diapir after bedding dip correction. (b) Stereonet displaying palaeostress orientations on the eastern flank of the diapir after bedding dip correction. (a) and (b) are from Figure 10i and Figure 10j respectively. After correcting for bedding, it is evident that σ_2 is perpendicular to the bedding surface, leaving σ_1 and σ_3 to become sub-parallel to the bedding surface. Majority of σ_1 orientations run in a north-south trend, whilst σ_3 runs in an east-west trend. Local variations do exist, however these cannot be confidently deduced as having a relationship with the diapir's location. It is unclear whether the Arumbera Sandstone bedding surface was level during diapir penetration, adding a limitation to the results.

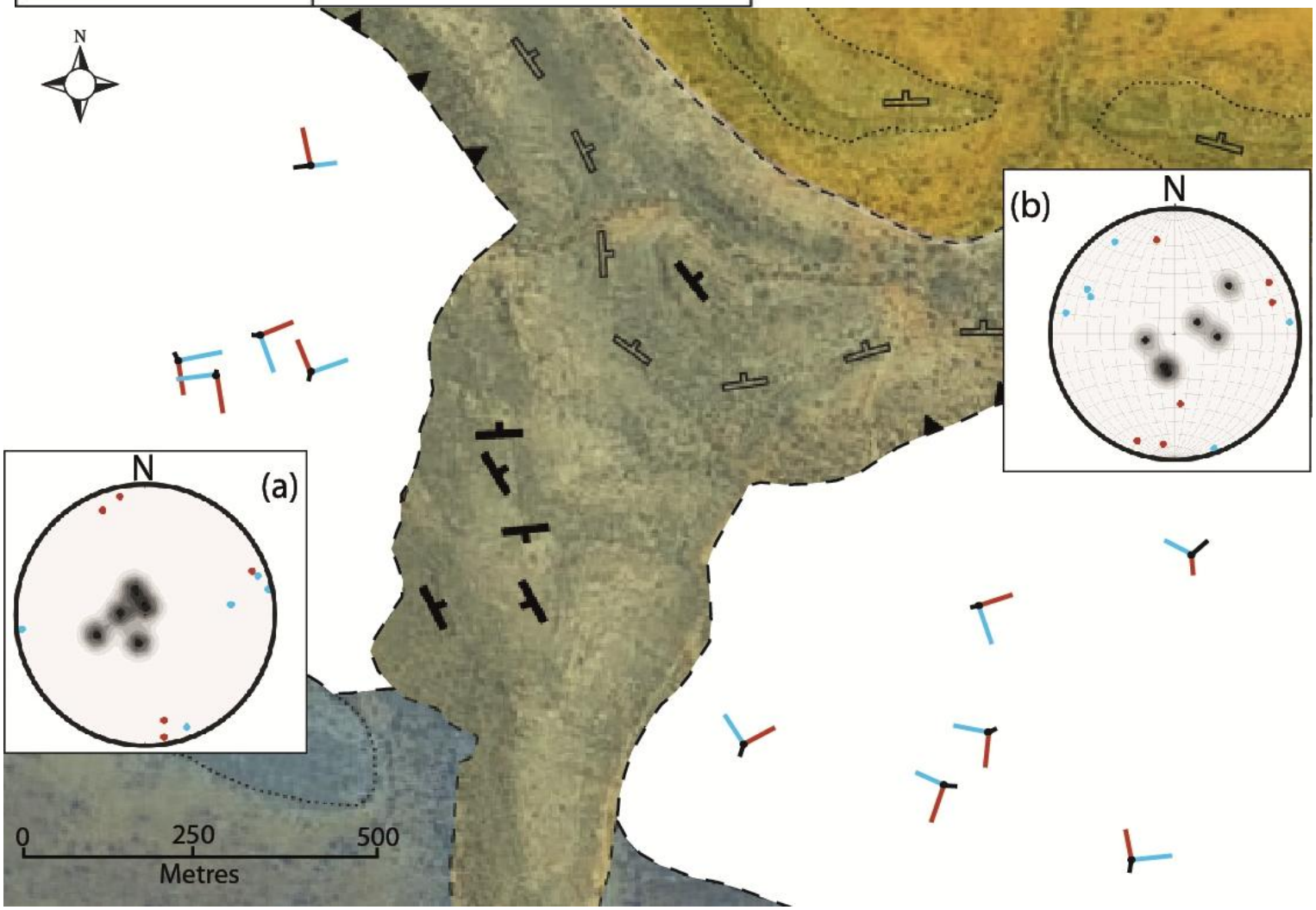

5. DISCUSSION

5.1 Gulf of Mexico Salt Diapirs

5.1.1 DIAPIR 1 (D1)

D1 is interpreted to have actively risen through overlying sediment (Nokes 2011). From this study it is determined that after the initial active diapir event, a close balance of passive and active diapirism still existed. This was demonstrated by onlap of syn-diapiric sediments against the walls of the diapir, suggesting that deltaic sediment has been deposited throughout the duration of diapiric rise. Fault interpretation from the east-west section (Figure 5) displays evidence of subtle gravitational collapse features on both the eastern and western flanks of the diapir. The implication of net normal displacement from this interpretation is consistent with the hypothesis that σ_H orientations become locally rotated sub-parallel to the interface between salt and sediment (Bell 1996b, Yassir and Zerwer 1997, King et al. 2012). In response to the gravitational collapse structures on the eastern flank of D1, it is interpreted that a pop up structure has formed a further 3 kilometres east of the diapir (Figure 5). This could potentially be due to the transfer of stress from gravitational collapse, to shortening a few kilometres further away, analogous to a DDWFTB. On the north-south section of D1 (Figure 6), zones of chaotic seismic facies are attributed to short periods of active diapir movement. These zones suggest that turbidity currents and gravity flows were caused by an active diapir environment, resulting in the deposition of heterogeneous overburden.

5.1.2 DIAPIR 2 (D2)

On the north-south section of D2 (Figure 8), chaotic reflections are highlighted and again can be attributed to periods of active diapir movement. Due to its stratigraphic depth, this chaotic facies is interpreted to be from an older period of active diapirism compared to the chaotic seismic facies observed in Figure 6. Stratigraphically above the chaotic zone, the excellent example of short prograding reflections indicates a sediment transport direction trending away from the diapir (Figure 8c). Faults and fractures also indicate net normal displacement close to the diapir wall, suggesting that σ_H is deflected sub parallel to the diapir-sediment interface.

The east-west section of D2 (Figure 7) displays the relationship between itself and D1 and how this can affect the variability of the in-situ stress orientation. Whilst net normal displacement is clear on the western flank of D2, there is also evidence of a thrust event in close proximity to D2 and stratigraphically above the normal faults (Figure 7). This is interpreted to be caused by the normal displacement on the eastern flank of D1 resulting in local compression within the minibasin in close proximity to D2. This example indicates that whilst each diapir can be individually analysed for σ_H deflections, there is a lot to be considered when two diapirs are in close proximity as the in-situ stress relationship between the two adds a degree of complexity to the structural deformation. I suggest that in-situ stress will not only vary laterally due to diapirism, but there must also be a small degree of variation when considering the vertical aspect. In the case of D2 in Figure 7, one thrust displacement is interpreted out of seven displacements identified.

5.1.3 DIAPIR 1 (D1) AND DIAPIR 2 (D2) EVOLUTION SUMMARY

The Jurassic aged Louann Salt in the Gulf of Mexico was deposited as a result of a subsidence-driven marine transgression that spread over Mexico and the southern United States (Wilhelm and Ewing 1972, Jackson and Seni 1983). Post-salt stratigraphy includes a combination of carbonates, shales and deltaic turbidites deposited from the Middle Jurassic Challenger Carbonates through to the Holocene Mississippi Fan deep water turbidites (Rowan 1997). Since the Middle Jurassic, sediment loading has caused episodic basinward movement of salt, leading to large concentrations of salt masses (Wu et al. 1990). After a period of starved sedimentation, renewed rapid accumulation of sediment during the Neogene and Pliocene led to the formation of salt sheets and diapirs (Wu et al. 1990).

Differential compaction and loading of sediment is associated with the formation of salt diapirs (Rowan and Vendeville 2006). In the region of the 3D Ship Shoal seismic cube, it is interpreted that both D1 and D2 have actively pierced through post-salt stratigraphy due to a similar style of sediment compaction. Both D1 and D2 have similar structural characteristics and are in close proximity to each other. It is therefore assumed that D1 and D2 generally share the same structural evolution.

Firstly, an initial phase of active diapirism occurred. This is evident from the chaotic seismic facies that exists immediately stratigraphically above the top pre-diapiric sediment horizon (Figure 5). After this period of active movement, both diapirs grew passively, evident from the onlap of deltaic sediment against the walls of D2 (Figure 7). After continued passive diapirism, further sediment deposition contributed to

progressive downbuilding of the mini-basin between D1 and D2. This was associated with salt withdrawal from underneath the flanks of D1, causing the formation of normal faults that dip towards D1 (Figure 6). A second period of active diapirism is evident from zones of chaotic seismic facies on the flanks of D1 (Figure 6). This second period of active diapirism is also represented by short, prograding reflections that indicate a sediment flow direction away from D2 (Figure 8).

Extensional faults and fractures along the flanks of both D1 and D2 are apparent throughout their structural evolution. Rapid thickness change in sediment along the western flank of D2 indicates early syn-depositional normal fault movement (Figure 7); whilst younger extensional faults and fractures that also exist along the flanks of both D1 and D2 indicate that this style of deformation has been the case throughout the evolution of the diapirs (Figures 5, 7 and 8). The single thrust event along the western flank of D2 is a result of localised compression, demonstrating the complexity of in-situ stress when two salt diapirs are in close proximity.

5.2 Amadeus Basin Field Work

5.2.1 STRUCTURAL GEOMETRY AND THRUST RELATIONSHIP

The regional geometry of the lithological formations in the field area suggests that the structural evolution of the diapir is more complex than first thought. All three units dip and young towards the north. This basic yet fundamental field observation of the arrangement of units suggests that a large thrust exists at the boundary between the Bitter Springs Formation and the Arumbera Sandstone (Figure 13). This is evident as the Late Proterozoic Bitter Springs and Areyonga Formations have been placed on top

of the Late Proterozoic to early Cambrian Arumbera Sandstone. Whilst the geological map (Figure 2) of the field area portrays a typical plan view of salt diapir morphology, the existence of the thrust and ages of the units suggest a complex structural evolution. The implication that the diapir is associated with a large thrust negates the hypothesis that diapir movement was syn-depositional as any thrust related deformation in the northern Amadeus Basin post-dates the deposition of the Arumbera Sandstone (Korsch and Lindsay 1989). The inference that the salt diapir was not syn-depositional has a large impact on the validity of the palaeostress orientations that are corrected for bedding (Figure 15).

5.2.2 CONVOLUTED BEDS

Whilst an abundance of convoluted beds and some water escape structures were observed in the Arumbera Sandstone, the presence of these convoluted beds do not show the pattern expected for syn-depositional diapir movement. As the diapir is closely associated with a large thrust fault (inferring that diapir penetration post dates deposition of the Arumbera Sandstone), convoluted beds must then be attributed to tectonic movement that pre-dates the diapirism and large thrust fault in the field area.

Lindsay (1987b) states that mobilisation of the Bitter Springs Formation started shortly after deposition and has been relatively constant throughout most of the Late Proterozoic and early Palaeozoic. It has also been suggested that the Bitter Springs Formation acted as a major decollement surface during the Alice Springs Orogeny (Wells et al. 1965, Forman et al. 1967). Seismic shaking can cause repeated and extensive change to unconsolidated sediment (Bartsch-Winkler and Schmoll 1984), as is

the case with active and reactive diapirism. However, I propose that the convoluted bedding observed in the Arumbera Sandstone is due to syn-depositional normal fault graben movement. From a detailed seismic stratigraphic study (Lindsay 1987a), it is evident that the Arumbera Sandstone thickens dramatically towards the north and then thins abruptly at the present northern margin, implying a major bounding normal fault on the northern margin of the basin (Korsch and Lindsay 1989). There is no evidence for a trench forming during deposition of earlier formations, suggesting that the trench appeared immediately prior to or during deposition of the Arumbera Sandstone (Korsch and Lindsay 1989). As this is the case, the Arumbera Sandstone would have been subject to tectonic movement in the subsiding hanging wall adjacent to the basin-bounding normal fault. My suggestion is that the convoluted beds and water escape structures in the Arumbera Sandstone are related to syn-depositional normal fault movement, as described by Korsch and Lindsay (1989), and not by active salt-diapirism within the Bitter Springs Formation.

5.2.3 PALAEOCURRENT

The geological map shows interpreted palaeocurrent directions from field measurements (Figure 2). Due to the structural trend of the Arumbera Sandstone and the average dip, palaeocurrent measuring points to the south are from older stratigraphy compared to measuring points towards the north. This accounts well for the variation in palaoecurrent direction as the sediments were likely to be deposited in a coastal or delta plane setting (Lindsay 1987a), implying that current direction would have varied extensively with changing deltaic conditions. Expected palaeocurrent directions that are associated with syn-depositional diapir movement would characteristically trend away

from the diapir's position. Although at a larger scale, this concept is clearly demonstrated by the short prograding reflections associated with D2 in the Gulf of Mexico (Figure 8). In the field however, because of the ambiguity of the palaeocurrent observations, no general trend can be attributed to salt diapirism. This is consistent with the argument that the diapiric event occurred well after deposition of the Arumbera Sandstone.

5.2.4 STRUCTURAL DEFORMATION AND PALAEOSTRESS

Outside of the salt diapir, the Bitter Springs Formation bedding orientation to the north of the field area conforms well to the Areyonga Formation and the regional trend. However, within the diapir and towards the sediment-diapir interface, where high levels of brecciation are evident, bedding is much harder to distinguish. It is evident here that active diapir movement has destroyed the thin laminations of the Bitter Springs Formation as it has actively pierced into the Arumbera Sandstone (Figure 11). The non-systematic nature of bedding orientations and brecciation of the Bitter Springs Formation within the diapir helps to confirm that the Bitter Springs Formation did actively pierce through the Arumbera Sandstone.

Palaeostress orientations from conjugate fractures in the Arumbera Sandstone show a large degree of variation with geographic position. From a plan view of the field area, it is difficult to confidently determine any stress rotations or deflections that are related to diapir proximity (Figure 14). If anything, the subtle rotation of σ_1 on the western flank of the diapir, from an approximately north to a northwest trend, may suggest that small local deflections are attributed to the salt diapir. This inference is limited however by

the large variation that the rest of the data displays, so it cannot be confirmed by any other physical examples. The observation that σ_2 is perpendicular to bedding is the most clarified result as this is consistent with a strike-slip fracture setting, as was determined from slickenline orientations. The σ_1 and σ_3 orientations having sub-parallel trends to the bedding surface is also consistent with the inference that σ_2 is perpendicular to bedding. The major caveat to the palaeostress analysis is that it is unclear what orientation the sedimentary layers of the Arumbera Sandstone were at when diapirism took place.

The Alice Springs Orogeny involved southward, Carboniferous aged, thrusting of the Arunta Inlier over the northern margin of the Amadeus Basin (Sandiford and Hand 1998). The implication of this is that natural fracture systems that are inherent from the Alice Springs Orogeny should have structural characteristics consistent with σ_1 having a north-south orientation. Significant folding due to shortening can complicate this. Berry et al. (1996) looked at natural fractures within the Palm Valley gas field in the Amadeus Basin and concluded that the fractures originated as a result of folding. Photo interpretation study of the Palm Valley anticline revealed two major fracture sets: a NNW-striking set and an ENE-striking set (Gillam 2004). The proposed model for these natural fractures accounts for variation of in-situ stress orientations. On the limbs of the anticline, local compression occurs during folding. Comparatively, on the fold hinge, local extension occurs (Berry et al. 1996, Gillam 2004).

Whether the Arumbera Sandstone in the field area lays on the limb of a fold is unclear. However, σ_1 orientations sub-parallel to the bedding surface, which have a north-south

orientation, are observed from natural fractures in the Arumbera Sandstone (Figure 15). I propose that these palaeostress orientations are a result of deformation from the north-south shortening associated with the Alice Springs Orogeny. Palaeostress orientations from the field study that disagree with this are due to local deflections caused by the salt diapir, although, the data obtained is not robust enough to infer a consistent trend of deflection.

5.2.5 FIELD AREA AND DIAPIR EVOLUTION SUMMARY

The geological evolution of the field area, including the salt diapir, can be deduced from the sedimentary characteristics observed and the structural data recorded. The Bitter Springs Formation in the field area was deposited between 700 and 800 Ma (Lindsay 1987b) in a low energy, hypersaline environment resulting in a combination of evaporites and carbonates with fine (0.5 cm) laminations. The Bitter Springs Formation was then buried by further sedimentation of shallow marine sands, silts and carbonates, including the Late Proterozoic Areyonga Formation and the Late Proterozoic to early Cambrian Arumbera Sandstone. Diapirism of the Bitter Springs Formation in the Amadeus Basin occurred soon after deposition in the Late Proterozoic (Lindsay 1987b). However, it is evident from field data that the diapir in this study was not syn-depositional. Convoluted bedding within the Arumbera Sandstone is attributed to seismic shaking associated with a large bounding normal fault that formed on the northern margin of the Amadeus Basin during deposition (Lindsay 1987a, Korsch and Lindsay 1989).

In-Situ Stresses Around Salt Diapirs

Due to its geomechanical properties, salt is incompressible and acts as a Newtonian fluid over geological time (Hudec and Jackson 2007). Hence, the Bitter Springs Formation has mobilised and acted as a detachment during the Alice Springs Orogeny (Wells et al. 1965, Forman et al. 1967). The salt diapir in the field area is therefore likely to have formed in response to thrusting that occurred during the Alice Springs Orogeny. I believe it formed as a reactive diapir due to the Areyonga Formation being thrust onto the Arumbera Sandstone (Figure 13). This major thrust fault exists at the boundary between the Arumbera Sandstone and the Bitter Springs Formation at the base of the salt diapir (Figure 2). I suggest that the salt diapir pierced through the thrust fault and intruded into the Arumbera Sandstone due to the mobilisation of the Bitter Springs Formation during the compressive tectonic stress regime of the Carboniferous Alice Springs Orogeny.

Palaeostresses observed from conjugate fractures in the Arumbera Sandstone which display a north-south σ_1 orientation are therefore regarded as deformational characteristics attributed to the Alice Springs Orogeny. Palaeostresses observed that are deflected to dissimilar orientations are due to complex perturbations of the transpressional in-situ stress regime associated with the Alice Springs Orogeny, caused by the presence of the reactive salt diapir.

For the Bitter Springs Formation to pierce through the Arumbera Sandstone at this particular location, an explanation needs to be considered as to what caused this point of weakness in the Arumbera Sandstone. Two alternative hypotheses to the structural evolution of the diapir can be deduced. Firstly the structural evolution may involve the

presence of a kilometre scale transpressional jog. For this to have occurred, the location of the diapir would have been the focus of transpressional deformation, supplying a zone of weakness for the Bitter Springs Formation to intrude. Secondly, the thrust fault on either side of the diapir may have at one point been disconnected, separated by a compressional relay zone at the location of the salt diapir. This hypothesis also provides an area where deformation may have been focussed, supplying a zone of weakness for diapir penetration.

With further field work, the inference that the salt diapir in the field area is reactive and associated with a large thrust fault can be either confirmed or negated. More complex multiple working hypotheses such as the transpressional jog and the compressional relay zone should be taken into consideration when exploring the possibilities for the evolution of the salt diapir. Future study would need to include more thorough data collection to help gain a larger data base of structural measurements. Field work should also extent along strike of the large thrust fault to help gain a better understanding of the nature of the detachment between the Arumbera Sandstone and the Areyonga Formation.

5.3 Limitations

5.3.1 SEISMIC INTERPRETATION

Sedimentary and structural deformation analysis of salt diapirs in the Gulf of Mexico is first and foremost an interpretation of 3D seismic data and is subjective to the interpreter (e.g. Bond et al. 2007). The resolution and quality of the data limits the detail of structural interpretation that can be made. This problem is apparent in close

proximity to the sediment-salt interface. Zones of poor seismic quality close to the diapir walls and crest are attributed to highly pervasive fracturing which cannot be resolved. The small faults and fractures that have been interpreted and used to infer in-situ stress are much larger in scale than what is seen in the Amadeus Basin. Whilst this study makes use of a 3D volume of data, only north-south and east-west sections were used for interpretation. Using composite lines would introduce different visual perspectives and assist in understanding the spatial complexity of small faults and fractures.

5.3.2 FIELD WORK

Structural measurements in the Amadeus Basin field area will have a small degree of inaccuracy due to human error. Adding to this, measurements were restricted to outcrops that lay along transects. A thorough collection of structural measurements across the whole field would produce a more reliable result, particularly for palaeostress analysis. Where possible, the most acceptable examples of conjugate fractures were used to infer palaeostress. However, it cannot be certain whether all of these fracture pairs are a result of conjugate fracturing, or exist due to separate deformational events that overprint each other and possess the ideal angular relationship by coincidence. Rare examples existed of fractures that were offset by up to 15 centimetres by other fractures of perpendicular strike. Although sparsely observed, this could suggest two periods of fracturing, further questioning the credibility of the conjugate sets used for this study. These offset characteristics however are only in the rare case and may result from movement during exhumation.

6. CONCLUSIONS

The purpose of this study was to assess the deflection of in-situ stress in close proximity to salt diapirs using 3D seismic data from the Gulf of Mexico and field structural observations from the Amadeus Basin, central Australia. After seismic interpretation of D1 and D2 from the Gulf of Mexico (Figures 5, 6, 7 and 8), it is evident that these salt diapirs have actively risen through deltaic sediment and were not associated with any large scale faults. Deformation characteristics such as gravitational collapse on the flanks of D1 and D2 imply net normal displacement. This is consistent with the hypothesis that σ_H becomes locally deflected sub parallel to the salt-sediment interface of diapirs. Similarities can also be drawn between these characteristics observed on the Gulf of Mexico seismic data and sediment drag zones, as modelled by Alsop et al., (2000) (Figure 3).

The salt diapir in the Amadeus Basin field area is within a much more complex structural setting compared to the Gulf of Mexico and is associated with a large NW-SE striking thrust fault (Figure 2). This implies that it has reacted to north-south shortening from the Alice Springs Orogeny, which post-dates sedimentation of the Arumbera Sandstone, negating the hypothesis that diapir movement was syn-depositional. Palaeostress analysis from conjugate pairs of fractures in the field area reveals a large variation in orientations for σ_1 and σ_3. However, σ_2 is consistently sub-perpendicular to bedding, thus σ_1 and σ_3 orientations are restricted to the plane of bedding. This observation of palaeostress implies that the fracture network in the Arumbera Sandstone is the result of a strike-slip regime. A definitive palaeostress deflection trend cannot be

drawn from the field data. Thus, the results from the field structural analysis are dissimilar to seismic interpretation from the Gulf of Mexico. Adding to this is the inconsistency with the style of diapirism between the two geological settings. The one major similarity is the result that the in-situ stress orientation in close proximity to salt diapirs can be more complex than first suggested. This is particularly the case when two diapirs are in close vicinity, as shown from the close occurrence of fractures with normal and reverse offset in the Gulf of Mexico (Figure 7).

The deflection of σ_H orientations to become sub-parallel to the salt-sediment interface has significant implications for stable drilling directions when exploring for hydrocarbons in close proximity to salt diapirs. In general, the most stable wells are those drilled in a direction that "feels" the least stress anisotropy. For example, in a normal fault stress regime ($\sigma_v > \sigma_H > \sigma_h$), such as the Gulf of Mexico delta top, the least stress anisotropy will be between σ_H and σ_h or between σ_v and σ_H, so vertical and horizontal wells drilled toward σ_h will be the most stable, respectively. Horizontal wells drilled toward σ_H will be the least stable. Thus, where we know stress orientations to deflect away from the regional predicted orientations around salt diapirs, stable well predictions become much more complex and a full understanding of these deflections is required.

This study has shown that in-situ stress deflections along the flanks of salt diapirs are associated with complex perturbations. These apparent deflections are dependent on the structural setting of each salt diapir and whether it is interpreted as active, passive or reactive.

ACKNOWLEDGMENTS

Kind thanks are due for the many staff and fellow students who assisted with my honours project, including fieldwork, peer reviews and general support:

Dr. Rosalind King

Dr. Kathryn Amos

Dr. Bruce Ainsworth

Lewis Maxwell

Nicholas Lyons

Courtney Fields

Dr. Simon Holford

Dr. Mark Tingay

Dr. Katie Howard

David Tassone

Ernest Swierczek

REFERENCES

ALSOP G. I.*, et al.* 2000 The geometry of drag zones adjacent to salt diapirs, *Journal of the Geological Society, London,* vol. 157, pp. 1019-1029.

BARTSCH-WINKLER S. & SCHMOLL H. R. 1984 Bedding types in Holocene tidal channel sequences, Knik Arm, Upper Cook Inlet, Alaska, *Journal of Sedimentary Petrology,* vol. 54, no. 4, pp. 1239-1250.

BELL J. S. 1996a In situ stresses in sedimentary rocks (part 1): measurement techniques, *Geoscience Canada,* vol. 23, no. 2, pp. 85-100.

--- 1996b In situ stresses in sedimentary rocks (part 2): applications of stress measurements, *Geoscience Canada,* vol. 23, no. 3, pp. 135-153.

BERRY M. D., STEARNS D. W. & FRIEDMAN M. 1996 The development of a fractured reservoir model for the palm Valley gas field, *APPEA Journal,* vol. 36, pp. 82-103.

BLACK L. P., SHAW R. D. & OFFE L. A. 1980 The age of the Stuart Dyke Swarm and its bearing on the onset of late Precambrian sedimentation in central Australia, *Journal of the Geological Society of Australia,* vol. 27, pp. 151-155.

BOND C. E.*, et al.* 2007 What do you think this is? "Conceptual uncertainty" in geoscience interpretation, *GSA Today,* vol. 17, no. 11, pp. 4-10.

COLLINS W. J. & SHAW R. D. 1994 Geochronological constraints on orogenic events in the Arunta Inlier: a review, *Precambrian Research,* vol. 71, pp. 315-346.

DOOLEY T. P., JACKSON M. P. A. & HUDEC M. R. 2007 Initiation and growth of salt-based thrust belts on passive margins: results from physical models, *Basin Research,* vol. 19, pp. 165-177.

FIDUK J. C.*, et al.* 1999 The Perdido Fold Belt, Northwestern Deep Gulf of Mexico, Part 2: Seismic Stratigraphy and Petroleum Systems, *AAPG Bulletin,* vol. 83, no. 4, pp. 578-612.

FORMAN D. J., MILLIGAN E. N. & MCCARTHY W. R. 1967 Regional geology and structure of the northeastern margin, Amadeus Basin, Northern Territory, *Geology and Geophysics,* vol. 103.

GALLOWAY W. E. 1989 Genetic Stratigraphic Sequences in Basin Analysis II: Application to Northwest Gulf of Mexico Cenozoic Basin, *AAPG Bulletin,* vol. 73, no. 2, pp. 143-154.

GALLOWAY W. E.*, et al.* 2000 Cenozoic depositional history of the Gulf of Mexico basin, *AAPG Bulletin,* vol. 84, no. 11, pp. 1743-1774.

GE H., JACKSON M. P. A. & VENDEVILLE B. C. 1997 Kinematics and Dynamics of Salt Tectonics Driven by Progradation, *AAPG Bulletin,* vol. 81, no. 3, pp. 398-423.

GILLAM D. J. 2004 Structural and Geomechanical Analysis of Naturally Fractured Hydrocarbon Provinces of the Bowen and Amadeus Basins: Onshore Australia. Australian School of Petroleum*.* pp. 292. The University of Adelaide.

HUDEC M. R. & JACKSON M. P. A. 2007 Terra infirma: Understanding salt tectonics, *Earth-Science Reviews,* vol. 82, pp. 1-28.

JACKSON M. B. A., VENDEVILLE B. C. & SCHULZ-ELA D. D. 1994 Salt-related structures in the Gulf of Mexico: A field guide for geophysicists. Bereau of Economic Geology*.* The University of Texas at Austin.

JACKSON M. P. A. & SENI S. J. 1983 Geometry and evolution of salt structures in a marginal rift basin of the Gulf of Mexico, east Texas, *Geology,* vol. 11, pp. 131-135.

JACKSON M. P. A. & TALBOT C. J. 1986 External shapes, strain rates, and dynamics of salt structures, *Geological Society of America Bulletin,* vol. 97, pp. 305-323.

KENNEDY M. 1993 The Undoolya Sequence: Late Proterozoic salt influenced deposition, Amadeus Basin, central Australia, *Australian Journal of Earth Sciences,* vol. 40, pp. 217-228.

KENT P. E. 1979 The Emergent Hormuz Salt Plugs of Southern Iran, *Journal of Petroleum Geology,* vol. 2, no. 2, pp. 117-144.

KING R. & BACKE G. 2010 A balanced 2D structural model of the Hammerhead Delta-Deepwater Fold-Thrust Belt, Bight Basin, Australia, *Australian Journal of Earth Sciences,* vol. 57, pp. 1005-1012.

KING R.*, et al.* 2012 Stress deflections around salt diapirs in the Gulf of Mexico, *Geological Society, London, Special Publications,* vol. 367, pp. 141-153.

KING R. C.*, et al.* 2009 Present-day stress and neotectonic provinces of the Baram Delta and deep-water fold thrust belt, *Journal of the Geological Society,* vol. 166, pp. 197-200.

KORSCH R. J. & LINDSAY J. F. 1989 Relationships between deformation and basin evolution in the intracratonic Amadeus Basin, central Australia, *Tectonophysics,* vol. 158, pp. 5-22.

LINDSAY J. F. 1987a Sequence Stratigraphy and Depositional Controls in Late Proterozoic-Early Cambrian Sediments of Amadeus Basin, Central Australia, *AAPG Bulletin,* vol. 71.

--- 1987b Upper Proterozoic evaporites in the Amadeus basin, central Australia, and their role in basin tectonics, *Geological Society of America Bulletin,* vol. 99, pp. 852-865.

MCCLAY K., DOOLEY T. P. & ZAMORA G. 2003 Analogue models of delta systems above ductile substrates *Geological Society, London, Special Publications,* vol. 216, pp. 411-428.

MORLEY C. K. 2009 Growth of folds in a deep-water setting, *Geosphere,* vol. 5, no. 2, pp. 59-89.

NOKES C. R. 2011 Finite numerical modelling of stress deflections around salt diapirs in the Gulf of Mexico. School of Earth and Environmental Sciences. The University of Adelaide.

ROWAN M. G. 1997 Three-dimensional geometry and evolution of a segmented detachment fold, Mississippi Fan foldbelt, Gulf of Mexico, *Journal of Structural Geology,* vol. 19, no. 3-4, pp. 463-480.

ROWAN M. G. & VENDEVILLE B. C. 2006 Foldbelts with early salt withdrawal and diaprism: Physical model and examples from the northern Gulf of Mexico and the Flinders Ranges, Australia, *Marine and Petroleum Geology* vol. 23, pp. 871-891.

SANDIFORD M. & HAND M. 1998 Controls on the locus of intraplate deformation in central Australia, *Earth and Planetary Science Letters,* vol. 162, pp. 97-110.

WELLS A. T., FORMAN D. J. & RAMFORD L. C. 1965 The geology of the north-western part of the Amadeus Basin, Northern Territory. Bureau of Mineral Resources, Australia.

WILHELM O. & EWING M. 1972 Geology and History of the Gulf of Mexico, *Geological Society of America Bulletin,* vol. 83, pp. 575-600.

WU S., BALLY A. W. & CRAMEZ C. 1990 Allochthonous salt, structure and stratigraphy of the north-eastern Gulf of Mexico. Part II: Structure, *Marine and Petroleum Geology,* vol. 7, pp. 334-370.

YASSIR N. A. & ZERWER A. 1997 Stress Regimes in the Gulf Coast, Offshore Louisiana: Data from Well-Bore Breakout Analysis, *AAPG Bulletin,* vol. 81, no. 2, pp. 293-307.

APPENDIX A: TABLE SUMMARY OF THE THREE TYPES OF SALT DIAPIRS (NOKES 2011)

Diapir Type	Characteristics
Reactive	• Triangular shape. • Size is controlled by the amount of regional extension. • Sediments bent upward approaching the salt diapir is due to subsidence of the flanks.
Active	• Discrete local extensional faulting is visible on seismic profiles. • Sedimentary roof is thinned by extensional faulting, fault blocks are dispersed outwards. • Roof strata slump off the domal bulge and along internal glide plains. • The strata displaced by slumping is accumulated and re-deposited next to the diapir. • Erosion can truncate all these structures, leaving an angular unconformity.
Passive	• Typically evolve to a steep sided, flat crested structure. • Surrounded by strata that show little faulting and thickness change. • Can revert back to active when sedimentation increases.

APPENDIX B: FIELD PALAEOSTRESS ANALYSIS DATA

Palaeostress	Stop #	Fracture Plane	Fracture Plane	σ1	σ2	σ3	Bedding Plane	Corrected σ1	Corrected σ2	Corrected σ3
West	37	284/54	186/60	346/15	241/45	098/40	010/38	348/07	248/56	083/33
	43	302/79	166/50	089/40	220/35	333/27	022/47	068/11	272/74	160/07
	48	317/60	192/72	090/45	263/46	356/02	-	-	-	-
	112	236/50	300/78	346/21	225/50	091/31	042/44	171/04	013/85	263/01
	113	227/43	302/78	347/15	235/50	090/30	031/47	171/18	333/72	079/00
	46	108/90	249/34	313/44	198/24	090/36	023/48	338/13	193/72	071/08
East	21	201/40	143/59	090/25	204/40	336/39	000/44	072/18	257/71	161/01
	24	223/57	156/50	271/01	179/48	002/41	-	-	-	-
	26	137/50	089/80	011/40	168/46	269/10	008/52	186/12	063/73	281/12
	27	127/52	195/30	090/20	195/29	332/53	-	-	-	-
	29	186/50	096/59	021/32	150/44	271/28	012/42	199/10	094/61	294/27
	60	156/66	070/61	006/06	107/55	270/34	001/48	175/42	049/41	297/22
	69	183/36	275/70	333/44	199/34	091/24	031/30	349/24	189/64	084/07
	79	249/24	120/60	089/48	200/15	302/35	023/52	062/14	198/68	327/13

APPENDIX C: FIELD TRANSECT LOCATIONS

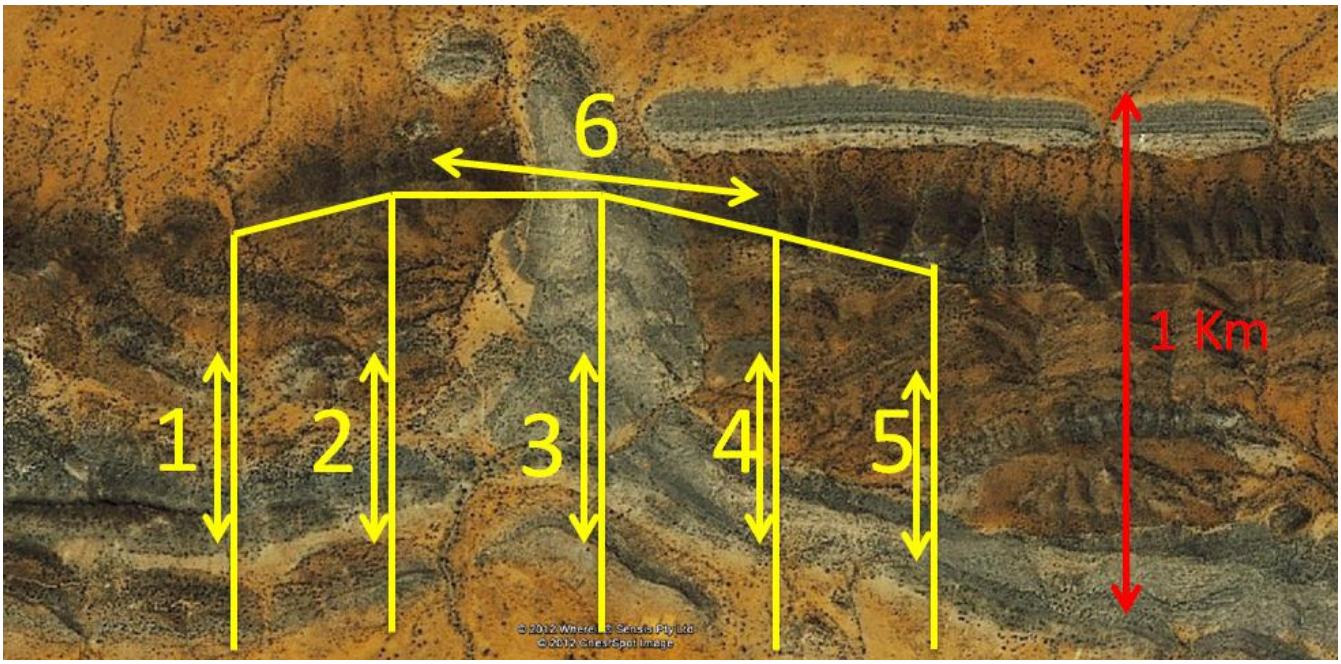

Appendix C: Landsat image of the Bitter Springs Formation (white) and the Arumbera Sandstone (brown-red). Yellow lines are field transects 1 to 6. Observations and measurements were recorded from the transect positions.